Journal of Statistical Mechanics: Theory and Experiment
An IOP and SISSA journal

PAPER: Classical statistical mechanics, equilibrium and non-equilibrium

Dynamical and structural properties of an absorbing phase transition: a case study from granular systems

R Maire*, A Plati, F Smallenburg and G Foffi*

Université Paris-Saclay, CNRS, Laboratoire de Physique des Solides, 91405 Orsay, France
E-mail: maire.raphael@yahoo.Fr and giuseppe.foffi@universite-paris-saclay.fr

Received 8 July 2025
Accepted for publication 19 November 2025
Published 16 December 2025

Online at stacks.iop.org/JSTAT/2025/123206
https://doi.org/10.1088/1742-5468/ae23bc

Abstract. We investigate the dynamical and structural properties of absorbing phase transitions within granular systems. Specifically, we examine a model for vibrofluidized systems of spherical grains, which undergo a transition from a state of purely vertical motion to one characterized by horizontal diffusion as the density increases. Numerical simulations reveal that, depending on the specific system parameters, both continuous and discontinuous transitions can occur, each associated with markedly distinct structural properties at the transition point. We explain this using a theoretical analysis based on kinetic theory applied to an effective 2D model, which elucidates the role of a synchronization effect in determining the nature of the transition. A fluctuating hydrodynamic theory, which quantitatively describes the structural and dynamical properties of the active state, such as hyperuniformity, is derived from the microscopic dynamics, together with an equilibrium-like assumption concerning the noises on the hydrodynamic fields. This work expands on previous studies by providing a comprehensive examination of the absorbing phase transition characteristics and proposing new theoretical models to interpret the observed behavior.

Keywords: absorbing states, granular material, kinetic theory of gases and liquids, numerical simulations

*Authors to whom any correspondence should be addressed.

Supplementary material for this article is available online

Contents

J. Stat. Mech. (2025) 123206

1. Introduction

In the context of non-equilibrium statistical physics, an *absorbing phase* occurs when a dynamical system is trapped in a stationary or periodic state in which no more evolution takes place. Upon variation of a suitable control parameter, a transition to a diffusive state can occur. Such transitions are termed absorbing phase transitions (APTs). The characteristics and universality class of these transitions have been extensively discussed in the literature [1, 2]. APTs have been observed in many different contexts, from epidemiology [3] to sandpile models [4–6], and from quantum systems [7–11] to chemical reactions [12]. Since the pioneering work by Pine *et al* [13], particle systems have also become a major area of study for APTs. Specifically, APTs have been observed in low Reynolds number reversible suspensions [13–18], dense colloidal systems [19–22], emulsions [23, 24], liquid crystals [25], glasses [26–28], jammed systems [29–31], granular materials [32, 33], chemical systems [34–36], ecology [37–40] materials at yielding [41] and turbulent systems [42–46].

In several of the cases mentioned above [13, 15, 16, 25, 31, 43, 47], the transition manifests in a continuous manner. This behavior has been interpreted within the framework of directed percolation [48] or conserved directed percolation models, notably the Manna models [49, 50]. These theoretical approaches have proven valuable in understanding the nature of the continuous transitions observed. However, a contrasting phenomenon has been documented in many other situations [17, 51–53]. In these instances, researchers have found that the transition exhibits a discontinuous character. To explain this divergence from the continuous behavior, it has been speculated that certain interactions might play a crucial role. Specifically, interactions potentially arising from hydrodynamic effects or material elasticity have been suggested as possible mechanisms that are responsible for the discontinuous nature of the transition [54].

Recently, we introduced a simple vibrofluidized granular model in which macroscopic spherical beads, confined within a quasi-2D cell, undergo a transition from a state in which they are locked in a vertical motion to a diffusive and active state in the horizontal direction as the density is increased [55]. Furthermore, by adjusting parameters such as the confinement height or the vibration amplitude, we showed that we can induce either a continuous or discontinuous transition. While continuous to discontinuous absorbing transitions have been observed in various systems [11, 37, 54, 56–61], the underlying physical explanations have often remained unclear. In our case, we demonstrated that this phenomenon was related to the synchronization between the vibrating cell and the vertical motion of the beads. The granular system under study was described using two different models: a realistic quasi-2D model, which can be numerically integrated using the discrete element method; and an effective model in 2D, which can be simulated through event-driven molecular dynamics and provides a good starting point for analytical investigations based on kinetic theory and hydrodynamics.

In this paper, we expand the scope of our previous investigation [55] in two primary directions. First, we examine the dynamical and structural properties of the absorbing phase transition, aiming to elucidate potential distinctions between continuous and discontinuous cases. Our analysis of the absorbing phase transition's properties focuses on identifying characteristic differences between continuous and discontinuous transitions.

J. Stat. Mech. (2025) 123206

This examination of dynamical and structural aspects aims to deepen our understanding of the underlying mechanisms driving these transitions and to draw connections with analogous phenomena in other systems. Second, we explore theoretical models that can interpret the observed phase transition by extending the kinetic theory framework we proposed in [55] and by proposing an approach grounded in fluctuating hydrodynamics to study the active state. These complementary theoretical frameworks offer valuable perspectives on the complex dynamics of the system under study.

The remainder of this paper is structured as follows. In section 2, we introduce and simulate the two models used to describe the granular system. In section 3, we compare, in greater detail, these two models close to the continuous and discontinuous transition by studying their structural and dynamical properties. This prepares the way for the kinetic theory discussed in section 4, which is then extended in section 5, using a hydrodynamics theory, allowing us to quantitatively predict the structural properties of the active phase.

2. APTs in a granular system

In this section, we describe two different numerical approaches used in the present study. First, we consider a realistic quasi-2D model, which is based on a detailed and accurate description of grain interactions and which includes the complete quasi-2D dynamics of the quasi-2D granular system. The advantage of this approach is that it models grain collisions in a more physically accurate manner, incorporating the mechanical properties of the materials involved. However, this approach turns out to be computationally very demanding. The second model we present is an effective 2D model that we have developed to simplify the problem [55]. This approach offers two significant benefits. These simulations become significantly less computationally demanding, enabling the exploration of time scales and system sizes increased by three orders of magnitude. Additionally, while our simplified model is approximate, it provides a better understanding of the underlying physical principles behind the observed phenomena and represents a more viable starting point for the analytical approach discussed later in the paper.

2.1. The realistic quasi-2D model

Our first model consists of a vertically vibrating granular system confined between two plates in a quasi-2D geometry (see figure 1). The evolution is simulated using molecular dynamics simulations based on the discrete element method [62, 63] using LAMMPS [64, 65]. This numerical approach is widely adopted to model realistic in-silico setups [66, 67], utilizing precise contact mechanics models [63, 68–70] for grain–grain and grain–plate interactions. These models encompass normal and tangential forces, capturing both their elastic and dissipative aspects. In particular, in this work, we adopt the Hertz–Mindlin contact model [71, 72]. Particles are also subject to a constant downward gravity field g.

In figure 1, we present a schematic diagram of the numerical setup. The simulation box has a square base of side L in the xy plane and height h, with $L \gg h$. Particles are confined in the z direction by two horizontal parallel plates, and periodic boundary

J. Stat. Mech. (2025) 123206

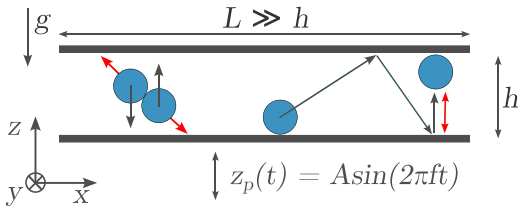

Figure 1. Numerical quasi-2D geometry used in realistic simulations. A vertical displacement $z_p(t)$ is imposed to the box to provide external energy to the system. Because of tangential frictional forces, the grains lose horizontal energy during collisions with the top and bottom walls. This mechanism introduces an effective dissipation rate $\bar{\gamma}$ for the horizontal dynamics. Energy transfer between the z and xy directions occurs during grain–grain non-planar collisions. This introduces an effective energy gain at collision for the xy motion.

conditions are imposed in the x and y directions. The grain–plate interaction includes tangential friction, which is crucial for the phenomenon under study.

The box vibrates in the z direction, following a sinusoidal equation of motion with frequency f and amplitude A: $z_p = A\sin(2\pi f t)$ and is filled with monodisperse spherical grains of spatial coordinates $\{x, y, z\}$, translational velocities $\{v_x, v_y, v_z\}$, angular velocities $\{\Omega_x, \Omega_y, \Omega_z\}$, diameter σ and mass m.

Within the LAMMPS simulations, these parameters are implemented in SI units, and we refer to [55] and its supplementary information for the numerical values of the physical properties of the beads and additional information concerning the simulations details.

During the simulation, the beads gain vertical (z) momentum and energy through the vibration of the plates. This energy is then distributed to the horizontal (xy) components of the momentum through collisions between the grains (as represented in the left-hand side of figure 1). Furthermore, energy is dissipated by tangential friction between the plates and the grains, which tends to slow the particles in between bead–bead collisions and eventually to completely arrest in the xy plane while still oscillating vertically. (see the right-hand side of figure 1).

We consider a system of N particles initialized with random velocities. At low densities, collisions are not frequent enough to convert the continuous supply of vertical energy into a horizontal one. Consequently, the system gradually cools due to friction with the plates until it becomes completely arrested in the xy plane, while still bouncing up and down along the z axis. We refer to this state as the absorbing state, as the system cannot escape the xy spatial configurations it has fallen into. At intermediate densities, the system reaches a horizontally active state in the xy plane, where the energy 'injected' during collisions is sufficient to balance the energy dissipated through tangential collisions with the plates. At very high densities, the system starts to crystallize [73–77] into an hexagonal phase and again reaches an 'absorbing phase' with 0 diffusivity in the xy plane, consistent with previous studies on APTs in cyclically sheared suspensions [13, 15, 31].

This qualitative picture is illustrated in figure 2, where the diffusivity in the xy plane is plotted as a function of the area fraction $\phi = \pi N\sigma^2/4L^2$. The diffusivity is given by

J. Stat. Mech. (2025) 123206

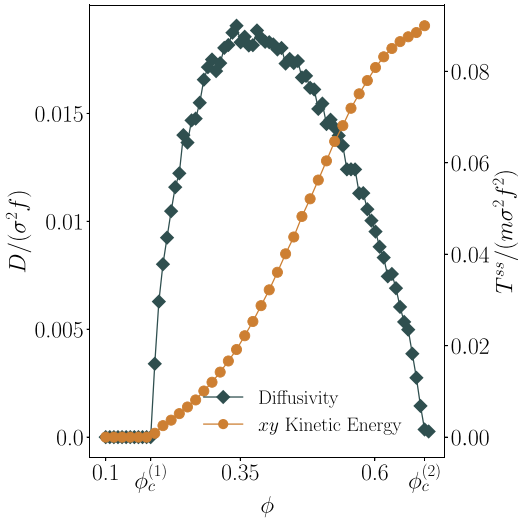

Figure 2. The mean diffusivity (rhombi) and horizontal kinetic energy (circles) as a function of the packing fraction for $h = 1.51\sigma$ and $A = 0.085\sigma$. Simulations are performed with $N = 10^3$ grains.

$D = \lim_{t\to\infty}\langle(\boldsymbol{r}_{xy}(t) - \boldsymbol{r}_{xy}(0))^2\rangle/4t$, where $\boldsymbol{r}_{xy}$ represents the horizontal coordinates of the position of a given particle, and $\langle\cdot\rangle$ refers to the average over all the grains. Indeed, at $\phi_c^{(1)}$, we observe the first transition, due to the competition between collision and dissipation, while at $\phi_c^{(2)}$, we observe the second re-entrant transition driven by cage formation and crystallization. In this paper, we focus entirely on the first transition, whose critical packing fraction will be simply denoted as ϕ_c.

To accurately characterize this transition, a more suitable order parameter is the mean horizontal kinetic energy of the grains:

$$T = \frac{1}{\mathcal{T}}\int_{t_0}^{t_0+\mathcal{T}} \frac{m}{2}\langle v_x^2(t) + v_y^2(t)\rangle \mathrm{d}t \tag{1}$$

where $\langle\cdot\rangle$ refers to the average over all the particles in an instantaneous configuration, t_0 is the initial measurement time and $\mathcal{T}$ is the observation time. This plays the role of a macroscopic effective temperature, sometimes called the granular temperature. We define T_{ss} as the steady-state temperature, obtained by choosing t_0 to be larger than any relaxation time in the system.

The behavior of T^{ss} is also presented in figure 2. Its value remains zero up to the absorbing-to-active transition at ϕ_c. Following this transition, the order parameter monotonically increases, which is in contrast to the non-monotonic trend observed for diffusivity due to the spatial localization of the particles at higher density [31]. The choice of T^{ss} as the order parameter will prove particularly suitable for the theoretical treatment we propose in section 4.

Interestingly, as discussed in [55], the nature of the transition as the packing fraction varies can be either continuous or discontinuous, depending on the values of physical

J. Stat. Mech. (2025) 123206

parameters, such as the amplitude of shaking or the height of the plate. This phenomenon was explained by an additional dynamical effect related to the synchronization of the beads with the moving plates. In what follows, we review and discuss this mechanism in detail.

From numerical simulations, we observe that an isolated particle, for a given set of parameters, can either begin oscillating in the z direction in phase with the plate (a state we call synchronized) after a characteristic time τ_{s}, or remain in chaotic motion, not synchronized with the plate. This crossover between periodic and chaotic dynamics for bouncing grains colliding with moving walls has already been observed in different experiments [78–83] and understood theoretically using simple dynamical models [84–86]. To quantify the degree of synchronization, we use the following parameter [87]:

$$s\left(t\right)=\left|\frac{1}{N}\sum_{j=1}^{N}\mathrm{e}^{\mathrm{i}\theta^{j}\left(t\right)}\right|, \tag{2}$$

where N is the number of particles, and θ^{j} is a 'phase' for particle j defined as:

$$\theta^{j}\left(t\right)=\frac{z^{j}\left(t\right)-z_{+}}{z_{+}-z_{-}}\mathrm{sign}\left(v_{z}^{j}\left(t\right)\right) \tag{3}$$

where z^{j} and v_{z}^{j} are the vertical position and velocity of the particle j,and $z_{+}=h+A-\sigma/2$ and $z_{-}=-A+\sigma/2$ are, respectively, the maximum and minimum z position. When all particles jump synchronously, they will coherently contribute to the sum in equation (2) and the synchronization parameter will be equal to one. For an asynchronized system, $s(t)$ will be lowered. We can now introduce the long-time average

$$s=\lim_{t_{0},t\to\infty}\frac{1}{t}\int_{t_{0}}^{t_{0}+t}s\left(t'\right)\mathrm{d}t' \tag{4}$$

to measure the degree of synchronization as a function of A and h. The resulting synchronization map is shown in the inset of figure 3(a).

This synchronization significantly impacts the energy exchange in the system. If two particles collide at the same height, no energy transfer between the vertical and horizontal degrees of freedom occurs, and the particles will undergo a purely dissipative collision in the xy plane. When most collisions occur between synchronized particles, the energy accumulated in the z direction is not distributed to the xy plane, causing the system to cool down and eventually enter an absorbing state. This has a profound effect on the nature of the transition that is exemplified in figure 3(a). In the region where the particles do not synchronize (green stars) we observe a continuous transition to the absorbing state. However, a slight change in the parameters (in this case, the amplitude A) yields the curve with the yellow square markers, which reaches an absorbing state at higher densities discontinuously because the particles for these parameters can synchronize with the plate (as seen in the inset). Roughly, the collision frequency of

J. Stat. Mech. (2025) 123206

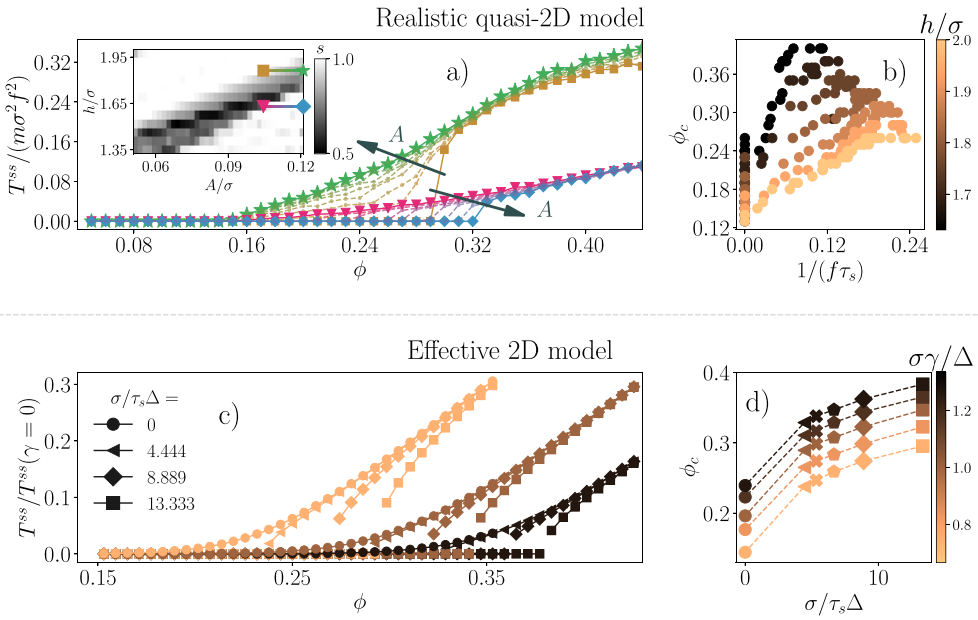

Figure 3. Comparison of the realistic quasi-2D model (a) and (b) with the effective 2D model (c) and (d). (a) Evolution of the xy temperature as a function of the density for various amplitudes and heights in the realistic quasi-2D model. The values of these parameters for each curve are indicated in the inset with corresponding markers. The inset is the synchronization map of the absorbing state with varying h and A. When the absorbing state is synchronized, the transition is discontinuous, while the opposite is observed when the absorbing state is chaotic. (b) The critical packing fraction as a function of $1/\tau_s$ in the realistic quasi-2D model. The synchronization time controls the packing fraction of the transition. (c) Temperature as a function of the packing fraction in the effective 2D model. Without synchronization ($1/\tau_s = 0$), the transition is continuous, while at finite τ_s, the transition is discontinuous (see, however, section 4.2 for a discussion of the existence of a tricritical point at finite τ_s). (d) The critical packing fraction as a function of the synchronization time for various damping in the effective 2D model. Consistently with the realistic model, the synchronization time increases the critical packing fraction since it facilitates the transition.

the last active steady state corresponds to the average time it takes for particles to synchronize τ_s. If the density is further lowered, particles have enough time to synchronize before colliding with others, leading to purely dissipative collisions in the xy plane and causing the system to cool to the absorbing state. This explains the sudden jump to the absorbing state observed for the curve with square or diamond markers compared to the stars and triangles.

It is important to note that synchronization of the particles requires a typical time τ_s, which plays a key role in determining the critical packing fraction ϕ_c where the transition takes place. This timescale can be tuned via the shaking amplitude and the sample height. To illustrate this, in figure 3(b) we plot the behavior of ϕ_c as a function of $(f\tau_s)^{-1}$ for a range of different conditions. We find that the critical packing fraction

J. Stat. Mech. (2025) 123206

measured for different amplitudes grows with the synchronization frequency $1/\tau_s$ at fixed h. As in [55], we measure τ_s for every A and h using an exponential fit of $s(t)$, starting from an asynchronized and absorbing state.

In summary, the observed phenomenology is attributable to the interplay between two distinct transitions: one between absorbing and active states in the xy-motion, and the other between synchronized and asynchronized states in the z dynamics. Without synchronization, the system continuously reaches an absorbing state due to tangential friction with the plate, while with synchronization, the transition is discontinuous and driven by purely dissipative collisions. Although it is possible to develop a theory for this system directly [88–93], we instead recall, in the following subsection, the model introduced in [55], which offers a simplified framework for analyzing the phenomenology observed in the more realistic setting.

2.2. The effective 2D model

In the preceding section, we have accumulated a wealth of information from the realistic quasi-2D model. Here, we will introduce an effective 2D model that incorporates the three primary mechanisms derived from the analysis of the realistic quasi-2D model. These mechanisms are: an effective dissipation rate for the horizontal motion, an effective parameter for the z-to-xy energy transfer at grain–grain collisions and a synchronization time τ_s. This simplified model will allow us to understand the interplay between APT and synchronization, and will rely on a minimal set of physical parameters compared to the realistic quasi-2D model.

The beads are modeled as identical hard disks of mass m and radius r undergoing dissipative collisions characterized by a coefficient of restitution α. In the realistic quasi-2D model, the energy is injected through vertical vibrations and subsequently converted into xy momentum through off-plane collisions. Brito *et al* [94] proposed a purely 2D model, effectively replicating the energy transfer mechanism of the realistic quasi-2D model by introducing the following collision rule between particles i and j:

$$\begin{aligned} \boldsymbol{v}_i' &= \boldsymbol{v}_i + \frac{1+\alpha}{2}\left(\boldsymbol{v}_{ij}\cdot\hat{\boldsymbol{\sigma}}_{ij}\right)\hat{\boldsymbol{\sigma}}_{ij} - \Delta_{ij}\hat{\boldsymbol{\sigma}}_{ij} \\ \boldsymbol{v}_j' &= \boldsymbol{v}_j - \frac{1+\alpha}{2}\left(\boldsymbol{v}_{ij}\cdot\hat{\boldsymbol{\sigma}}_{ij}\right)\hat{\boldsymbol{\sigma}}_{ij} + \Delta_{ij}\hat{\boldsymbol{\sigma}}_{ij}, \end{aligned} \tag{5}$$

where $0 \leqslant \alpha \leqslant 1$ is the coefficient of restitution, $\boldsymbol{v}_i'$is the post-collision velocity of particle i, $\boldsymbol{v}_i$ is its pre-collision velocity, and $\hat{\boldsymbol{\sigma}}_{ij} = (\boldsymbol{r}_j - \boldsymbol{r}_i)/|\boldsymbol{r}_j - \boldsymbol{r}_i|$ and $\boldsymbol{v}_{ij} = \boldsymbol{v}_j - \boldsymbol{v}_i$ are the unit vector joining particles i and j and the relative velocity between them, respectively.

The last term in equation (5) accounts for energy injection, with $\Delta_{ij} > 0$ ensuring that energy input from this term remains positive at each collision, thus reproducing the conversion of vertical motion into horizontal motion in the realistic quasi-2D system. However, the collision can still be dissipative if the relative velocity is large. The Δ_{ij} is an effective parameter that takes into account the effects of the height of the plate and the driving on the energy transfer at collision on a coarse level. We will show that it can be chosen to depend on the degree of synchronization of the particles.

J. Stat. Mech. (2025) 123206

Furthermore, in the realistic quasi-2D model, the beads lose energy upon collisions with the ceiling or bottom of the plate. To incorporate this effect in our effective 2D model, we introduce a viscous drag γ during the free flight between collisions:

$$\frac{\mathrm{d}\boldsymbol{v}_i}{\mathrm{d}t} = -\gamma \boldsymbol{v}_i. \tag{6}$$

For the fixed parameters α, γ and Δ, the system can exhibit either an absorbing state or an active state, depending on density. At low density, the dynamics are primarily governed by viscous drag, causing the system to eventually come to rest in an absorbing state. In contrast, at high density, the dynamics are mainly driven by collisions, leading the system to an active steady state. It should be stressed that, up to this point, the dynamics we consider are very close to those introduced in [95].

To model the dynamics observed with the realistic quasi-2D model, we must incorporate synchronization into our effective 2D model as well. In the realistic quasi-2D model, simulations of free (non-colliding) particles with random initial conditions demonstrate a tendency to synchronize with the plate after a randomly distributed time interval τ_s. Moreover, we recall that collisions between the particles disrupt their synchronization, as these collisions effectively randomize the post-collision vertical velocity. Even in-plane collisions between synchronized particles slightly asynchronize them over a timescale τ_s', which is, on average, significantly shorter than τ_s. To easily incorporate all these aspects of the realistic quasi-2D model into our model, we make the assumption that a single constant synchronization time, denoted as τ_s, is sufficient to qualitatively describe the synchronization. In the effective 2D model, particles are either labeled as synchronized or asynchronized. Free flight lasting more than τ_s synchronizes the particle, while any collisions desynchronize it.

We recall that this synchronization effect plays a major role in the energy transfer at collision. In the realistic quasi-2D model, since synchronized particles colliding have the same z coordinate, no transfer of vertical kinetic energy to the horizontal degrees of freedom occurs. Asynchronized collisions are instead mostly non-planar, causing a significant z-to-xy energy transfer. To capture this behavior in our existing effective 2D model, we define a synchronization-dependent Δ_{ij}. If both particles involved in a collision have not had a collision for a time period longer than τ_s, the collision does not add energy to the system, i.e. we set $\Delta_{ij} = 0$. For all other collisions, where at least one of the particles involved has had a collision within the last τ_s time period, we process the collision with a fixed $\Delta_{ij} > 0$, representing the transfer of energy and momentum resulting from asynchronized collisions.

Formally, the value of Δ_{ij} for a collision between particles i and j takes the form

$$\Delta_{ij} = \begin{cases} \Delta > 0 & \text{if } \delta t_i < \tau_\mathrm{s} \text{ or } \delta t_j < \tau_\mathrm{s} \\ 0 & \text{otherwise,} \end{cases} \tag{7}$$

with δt_i being the time since the last collision of particle i. Clearly, in the limit $\tau_\mathrm{s} \to \infty$, no synchronization takes place.

Event-driven molecular dynamics simulations [96] of this 2D model are performed with up to 1.5×10^7 particles in a square box with periodic boundary conditions. We

J. Stat. Mech. (2025) 123206

ensure that simulations are run long enough to let the system reach a steady-state temperature $T^{\rm ss}$. The system-wide granular temperature T of the 2D model, defined as in equation (1), will play the role of a mean-field order parameter and is the equivalent of the xy temperature defined for the realistic quasi-2D model. We again define the steady-state temperature $T^{\rm ss}$ as the temperature measured after the system has relaxed. As shown in figure 3(c), we observe that by setting $1/\tau_{\rm s} = 0$ (i.e. no synchronization, circular plot markers), the system undergoes a continuous transition as the packing fraction of particles is varied. However, once synchronization is introduced by setting $1/\tau_{\rm s} > 0$, a discontinuous transition is observed, in agreement with the results found in the realistic quasi-2D model. For fixed values of Δ and α, two timescales are in operation, as seen in figure 3(d). On the one hand, for a fixed value of $\tau_{\rm s}$, the critical packing fraction increases with the increasing drag coefficient γ. Indeed, higher drag implies that a denser system is needed to ensure sufficiently frequent collisions to sustain an active steady state. On the other hand, at a fixed value of γ, the critical packing fraction increases upon decreasing $\tau_{\rm s}$, as this makes it easier to synchronize and hence lose energy. Another way to look at this is through the frequency of collision. When synchronization is in operation in our system, we expect that at the critical packing fraction, the rate at which a particle synchronizes $1/\tau_{\rm s}$ is of the same order of the frequency of collision, which is itself, at a given temperature, an increasing function of ϕ.

3. Dynamical and structural properties of the phase transition

In this section, we examine the behavior of our system near the transition points. In particular, we highlight the differences between continuous and discontinuous transitions. Whenever possible, we also compare our findings with the behavior observed in similar systems reported in the literature.

3.1. Nature of the transitions

Thus far, we have discussed the APT in terms of a discontinuous or continuous transition, simply based on whether there is an obvious jump in kinetic energy as a function of the packing fraction. In this section, we take a closer look at the behavior around the transition point to examine the nature of the transition in more detail, for both the realistic quasi-2D and effective 2D model.

For continuous transitions, in systems characterized by an infinite number of absorbing states and a conserved number of particles without additional symmetries, the associated phase transition is believed to belong to the conserved directed percolation universality class [31, 95, 98, 99]. Evidence of this universality class, from the analysis of power-law scaling, is given in figure 4, where simulation results for both the realistic quasi-2D and the effective 2D models are compared to the expected results for systems belonging to the conserved directed percolation universality class. In particular, panels (a)–(c) present data of the realistic quasi-2D model, while (d)–(f) present those of the effective 2D model. In panels (a) and (d), we show that the order parameter variation, as a function of the distance from the critical point, obeys a power-law scaling characterized by an exponent very close to what is expected for the conserved directed

J. Stat. Mech. (2025) 123206

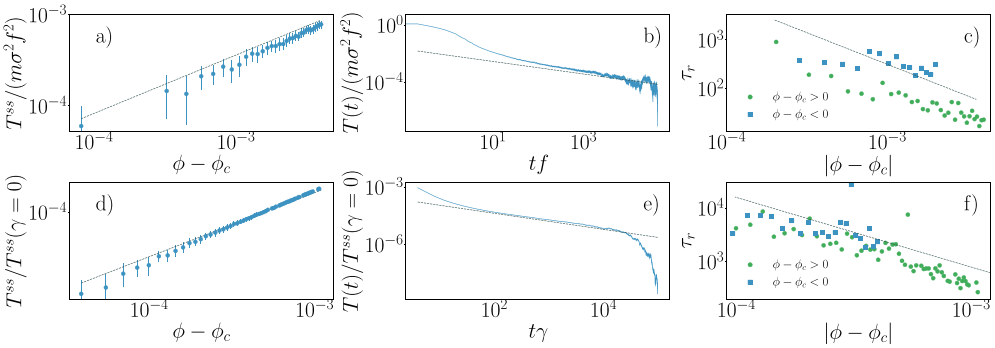

Figure 4. (a)–(c) The power-law behavior of observables for the realistic quasi-2D model with parameters $A = 0.085\sigma$, $h = 1.5077\sigma$ and $N = 30000$ leading to $\phi_c \simeq 0.186$. (d)–(f) The power-law behavior of observables for the effective 2D model with parameters $\Delta/(\sigma\gamma) = 0.15$, $\alpha = 0.95$ and $N = 10^6$ leading to $\phi_c \simeq 0.1509$. The dashed lines represent the power law expected from a 2D system belonging to the conserved directed percolation universality class [21, 97]. (a), (d) The order parameter as a function of $\phi - \phi_c$. The expected exponent $\beta \simeq 0.64$ with $T^{ss} \sim (\phi - \phi_c)^\beta$. (b), (e) The average over 100 runs of the evolution of the order parameter at ϕ_c. The expected exponent $a \simeq 0.42$ with $T(t) \sim t^{-a}$. (c), (f) The time to relax to the steady state as a function of $|\phi - \phi_c|$. The expected exponent $\gamma \simeq 1.3$ with $\tau_r \sim |\phi - \phi_c|^{-\gamma}$.

percolation universality class. In panels (b) and (e), we give the time evolution of the order parameter at the critical packing fraction ϕ_c. For the effective 2D model, the expected scaling closely matches the evolution of the order parameter. For the realistic quasi-2D model, however, it is more challenging to discern the correct scaling due to the limited simulation time and the difficulty in accurately pinpointing the transition point. In panels (d) and (f), we provide data for the characteristic time τ_r to reach the steady state. Above ϕ_c, τ_r is defined as the time at which the system first reaches its steady-state value within an arbitrary precision, which we set to 10 percent of the average steady-state temperature. These curves match the expected scaling well. Below ϕ_c, τ_r is defined as the first time the system reaches an arbitrarily small value. We find significant variations in the curves, depending on the chosen threshold, since the energy decreases as an exponential after the last collision. Here, we define the threshold as the lowest metastable steady-state temperature observed in a system that eventually decays to the absorbing state. Note that the measured exponent is known to be dependent on the initial conditions [97]. From the overall agreement with the expected scaling laws, we conclude that the phase transition is consistent with the conserved directed percolation universality class, although a definitive confirmation would require a finite size analysis.

It is worth noting that our focus has been on systems exhibiting their phase transition at a relatively high critical packing fraction ($\phi_c > 0.1$) [2, 95]. In contrast, when the transition occurs at very low ϕ_c, the system may exhibit mean-field conserved directed percolation critical exponents due to effectively long-range interactions, as discussed in [2, 95].

J. Stat. Mech. (2025) 123206

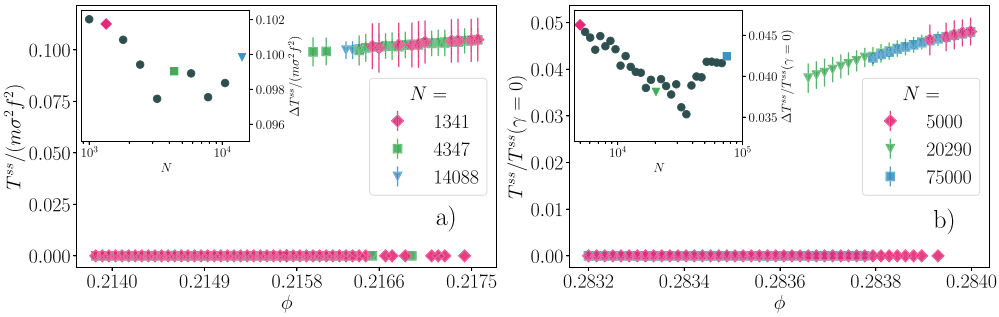

Figure 5. Comparison of the order parameter evolution as a function of the packing fraction in the realistic quasi-2D (a) and effective 2D model (b) for different system sizes. The main figures represent the evolution of the steady-state temperature in the discontinuous case (we recall that the temperature is the xy kinetic energy for the realistic quasi-2D model and the usual kinetic energy for the effective 2D model) for different system sizes, and the insets show the evolution of the order parameter of the last (the most dilute) active steady state ($\Delta T_{\rm ss}$) as a function of the system size. (a) For the realistic quasi-2D model: $A = 0.0626\sigma$ and $h = 1.95\sigma$. (b) For the effective 2D model: $\Delta/\gamma\sigma = 1.5, \alpha = 0.95$ and $1/\gamma\tau_{\rm s} = 16.67$.

Having clarified the nature of the continuous transition, we now turn to the discontinuous transition and perform a finite size analysis to prove that the finite discontinuity does persist in the infinite system size limit. We define $\Delta T_{\rm ss}$, which corresponds to the observed value of the order parameter of the most dilute system in the active state at a given system size and simulation time. For a continuous transition, we expect that at finite times, $\Delta T_{\rm ss}$ decreases with N and reaches 0 at infinite system size since the order parameter must vanish continuously. By contrast, for discontinuous transition, $\Delta T_{\rm ss}$ should not vanish. The evolution of the order parameter as a function of ϕ close to the discontinuous transition as well as $\Delta T_{\rm ss}$ as a function of the system size in the inset are given, for the realistic quasi-2D and effective 2D models in the insets of figures 5(a) and (b), respectively. Starting from a small system size, we see that increasing its size allows us to obtain a transition at a lower density, as would be expected as well for a continuous transition. However, beyond a given system size, $\Delta T_{\rm ss}$ ceases to decrease and instead increases with size, indicating a discontinuous jump in the order parameter in the thermodynamic limit and confirming the first-order nature of the transition.

We interpret such non-monotonic behavior of $\Delta T_{\rm ss}$ as nucleation dynamics—characteristic of discontinuous transitions—and better understood directly from the average time necessary for the system to reach an absorbing state at a given packing fraction in the metastable zone. We denote this time $t_{\rm wait}$ and study its behavior as a function of the number of particles for the effective 2D model in figure 6. The time $t_{\rm wait}$ acts as a proxy for the nucleation time, since the growth of the nucleus after it has reached its critical size should be fast compared to $t_{\rm wait}$. We only perform the analysis for the effective 2D model due to the prohibitive simulation time of the realistic quasi-2D model. For small system sizes, the waiting time increases with N since the fluctuation required for the system to reach an absorbing state is of the order of the size of the system. Then, the waiting time reaches a maximum, which corresponds to a

J. Stat. Mech. (2025) 123206

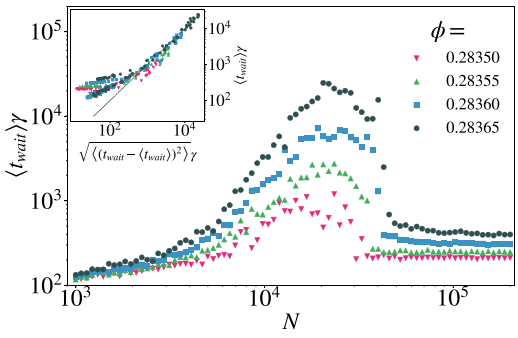

Figure 6. The waiting time in the effective 2D model for a system initialized in an active state to reach an absorbing state for different densities in the metastable zone; $\alpha = 0.95$, $1/(\tau_s\gamma) = 16.67$ and $\Delta/(\gamma\sigma) = 1.5$. The inset shows the average waiting time as a function of its standard deviation. The dashed line is a linear scaling, showing that the process is Poissonian. Each point corresponds to an average over 50 independent runs.

system size close to the size of the critical nucleus. It then decays due to the increase in available nucleation sites, until reaching a constant at larger system sizes due to the finite cooling rate imposed by γ and the frequency of collision. Note that the decrease in the waiting time for system sizes larger than the critical nucleus is very sharp, while in an equilibrium, we would expect a decay proportional to $1/N$. This might be the result of hydrodynamical instabilities or non-equilibrium structural properties at small k, inaccessible to small system sizes, which are common in granular systems [100–102]. Note also that contrary to equilibrium systems, the nucleation dynamics, and especially the growth of the nucleus, exhibit exotic behavior, both for the effective 2D and the realistic quasi-2D models. Since the order parameter is the activity or the temperature of the system, the nucleus cannot be stationary because, during its growth, active particles around it will quickly convert its inactive grains into active ones. We instead observe damped traveling waves of energy and density, slowly decreasing in amplitude until the absorbing state is reached (see Video 1 for the realistic quasi-2D model and Video 2 for the effective 2D model). Moreover, contrary to [33], we do not find a strongly diverging radius of the critical nucleus as we approach the stable fluid region but merely a strong increase in the effective energy barrier of nucleation. In the inset of figure 6, we confirm that the statistics of the waiting time are Poissonian when the reaching of the absorbing state is controlled by nucleation [103].

Interestingly, a very similar system has been studied by Lei, Hu and Ni [33, 53, 104–106]. They, however, found a different phenomenology. We provide additional discussions on this matter in appendix C.

3.2. Structural properties of the transitions

Having clarified the nature of the transition, we now focus on the dynamical and structural properties of the system close to it. In figure 7, we present, for both the effective 2D model and the realistic quasi-2D model, snapshots above and below ϕ_c for both

J. Stat. Mech. (2025) 123206

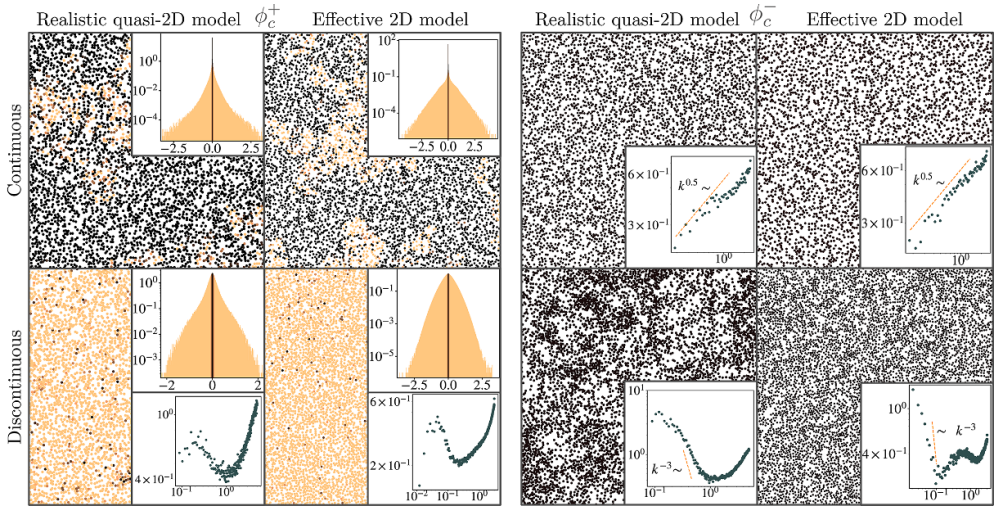

Figure 7. Zoomed snapshots of the systems above (ϕ_c^+, left) and below (ϕ_c^-, right) the critical packing fraction for the realistic quasi-2D and effective 2D models. The particles with small velocities are drawn in black. The insets above ϕ_c represent the velocity distribution of particles corresponding to the snapshots in units of Δ for the effective 2D model and σf for the realistic quasi-2D model. The colors of the histograms of velocities match those of the particles in the snapshots (inactive are in black, and active are in orange). The other insets represent the structure factor $\boldsymbol{S}_{\rho\rho}(k)$ of the corresponding snapshots as a function of the wavenumber in units of $1/\sigma$.

types of transition, and the probability distribution of the velocities in the diffusive phase, and the long-wavelength behavior of the structure factor in the absorbing phase.

In a continuous transition, the system reaches the absorbing state due to viscous drag forces. As commonly observed in similar situations, the critical point is characterized by avalanches of active particles that span the whole system [107–109]. This behavior is exemplified in the snapshots and leads to a distinctly identifiable population of inactive particles, discernible through the peak observed in the velocity distribution at the origin.

To examine the structure of our systems, we calculate the density structure factor, given by

$$S_{\rho\rho}(\boldsymbol{k}) = \frac{1}{N}\left\langle \sum_{j=1}^{N}\sum_{k=1}^{N} \mathrm{e}^{-\mathrm{i}\boldsymbol{k}\cdot\boldsymbol{r}_{jk}} \right\rangle. \tag{8}$$

Close to the transition point, $S_{\rho\rho}$ exhibits scaling behavior of the form $S_{\rho\rho}(|\boldsymbol{k}| \to 0) \sim k^{\nu}$, with $\nu \simeq 0.5$ [110]. The vanishing of the structure factor at $k = 0$ is called hyperuniformity [111–113] and is directly related to a suppression of density fluctuations on large length scales. This trend is consistent with the typical hyperuniform behavior observed at the critical point associated with the conserved directed percolation universality class [95, 114]. It has been observed that this scaling is expected to hold exactly at the transition point and to be lost below or above it [115]. In our models,

J. Stat. Mech. (2025) 123206

however, the system sizes are presumably not large enough for this hyperuniform scaling to break. Very recent works have successfully predicted hyperuniform scaling of the structure factor from a renormalization group approach by mapping the conserved directed percolation problem to the interface position at depinning for an elastic manifold [110]. A direct analysis of the hyperuniformity from the renormalization group of the conserved directed percolation field theory was also performed in [116] at the first loop.

Finally, we report new hyperuniform scaling for the longitudinal and transverse velocity fields at criticality in appendix B.

The velocity distributions in the active state exhibit peculiar scaling. As already noted, a finite portion of the system is almost completely inactive; hence, there is a sharp peak at $v = 0$, both for the realistic quasi-2D model and the effective 2D model to the velocity distribution. Moreover, at small velocity, we observe an exponential distribution with a non-trivial power: $\exp(-a|v|^{\delta})$ with $\delta \leqslant 1$, which then morphs into a simple exponential scaling, $\exp(-b|v|)$ at $v \simeq \Delta$. This effect is not surprising as non-Gaussian scalings are common in granular systems and, notably, it is known that the homogeneous cooling state exhibits a simple exponential tail while the homogeneously heated granular gas has an exponential tail with the exponent $\delta = 3/2$ [117–119]. In particular, a simple exponential tail appears frequently [120, 121] and is conjectured to be universal for systems with adiabatic energy changes. However, this is not the case in our system, since the energy change during a collision is large compared to the energy of the particles. In our case, the pronounced non-Gaussian behavior is most likely due to the finite jump processes affecting the velocities, effectively transforming the dynamics into a generalized Ornstein–Uhlenbeck process with discrete jumps of size $\pm\Delta$. This makes the system analogous to a stochastic resetting problem, where an overdamped particle in a harmonic potential is reset away from the origin. Such processes are known to asymptotically yield stationary distributions with exponential or power-law tails [122, 123]. In appendix A, we provide an explanation of this peculiar velocity distribution using an approximation for the Boltzmann equation.

In the discontinuous case, the system primarily transitions into the absorbing phase in a manner similar to the cooling behavior observed in a granular gas. This is because most of the energy is dissipated through collisions between synchronized particles, with the drag playing a secondary role in this process. Interestingly, the presence of viscous friction is not a prerequisite for observing a transition. While it helps the system to reach an absorbing state sooner, the dissipative character of synchronized collisions alone is sufficient to deplete the entire energy of the system in the infinite time limit. This implies the formation of clusters similar to those observed in the inhomogeneous cooling state [100, 124, 125] for the realistic quasi-2D model, as can be seen in the snapshots and from the upturn of the structure factor at $k \to 0$. A scaling close to k^{-3}, but less steep, is observed in the intermediate wavenumber region, which is roughly consistent with Porod's law [126, 127]. The inhomogeneous cooling is, however, arrested at a finite time due to the drag. In the effective 2D model, as collisions lead to a complete asynchronization of particles, the formation of clusters due to dissipative collisions is less prominent because high density regions of synchronized particles will quickly be shattered by any collision. However, even if the growth of the nucleus cannot proceed

J. Stat. Mech. (2025) 123206

as the beginning of the inhomogeneous cooling in the effective 2D model, Porod's law is approximately verified.

The active state of the discontinuous transition does not exhibit a population of inactive particles but still exhibits marked non-Gaussian behavior that, contrary to the continuous transition, can be in part attributed to the dissipative collisions. We also provide the structure factor of the fluid close to the metastable region, which is in itself interesting. Lei and Ni [105] observed a hyperuniform scaling $S \sim k^{1.2}$ in a metastable fluid at very small wavenumbers. As already mentioned, due to the dissipative collisions between synchronized particles, we instead observe a peak in the structure factor corresponding to the inverse average cluster size. We show in appendix C that without dissipative collisions ($\alpha = 1$) close to the metastable fluid, we recover a structure factor that is similar to that found by Lei and Ni.

4. Kinetic theory

In this section we develop the kinetic theory of the homogeneous state for the effective 2D model. We quantitatively predict the transition points and the steady-state temperature of our systems. We relate our findings to results already obtained in the literature.

4.1. Simple Δ model

Before introducing the theory of the full effective 2D model, it is useful to discuss the scenario where particles never synchronize, which corresponds to $\tau_s \to \infty$ and, consequently, $\Delta_{ij} = \Delta$ is constant, see equation (7). If the theory is accurate, it should predict, in this situation, a continuous transition. We first recall the theory developed in [55] and introduced in [94].

The temperature change of the system, assuming homogeneity, is only determined by the energy injection and dissipation following the relation

$$\frac{\partial T}{\partial t} = G(\phi, T), \tag{9}$$

where $G(\phi, T)$ represents the rate of energy change. The stable steady-state temperature T^{ss} is thus given by:

$$\begin{aligned} G(\phi, T^{\text{ss}}) &= 0, \\ \left.\frac{\partial G(\phi, T)}{\partial T}\right|_{T^{\text{ss}}} &< 0 \end{aligned}. \tag{10}$$

Here, G has two contributions: energy change due to collisions, and drag. It can be written as

$$G(\phi, T) = \frac{\omega(\phi, T)}{2} \langle E' - E \rangle_{\text{coll}} - 2\gamma T. \tag{11}$$

Here, the first term represents the change of energy due to collisions, calculated as the product of the frequency of collision $\omega(\phi, T)$ of a single particle, divided by 2 to avoid

J. Stat. Mech. (2025) 123206

double counting, with the average energy change during a collision, while the second term represents the drag.

Using the collision rule of the simple Δ model (equation (5)) and averaging over collisions, the energy change per collision can be estimated explicitly [94]:

$$G(\phi,T)=\frac{\omega_e(\phi,T)}{2}\left(m\Delta^2+\alpha\Delta\sqrt{\pi mT}-T\left(1-\alpha^2\right)\right)-2\gamma T, \tag{12}$$

where m is the mass of a particle. This result is based on the assumption of uncorrelated velocities (molecular chaos) and Gaussianity of the velocity distribution. The detailed calculations required to arrive at equation (12) can be found in [55]. These assumptions immediately imply that the frequency of collision is given by the so-called Enskog frequency of collision ω_e [128]:

$$\omega(\phi,T)=\omega_e(\phi,T)=\frac{\langle|\boldsymbol{v}|\rangle}{l(\phi)}=\frac{8\phi\chi(\phi)}{\sigma\sqrt{\pi m}}\sqrt{T}=\tilde{\omega}(\phi)\sqrt{T}, \tag{13}$$

where $l(\phi)$ is the mean free path, and χ is the Enskog factor taken to be the radial pair distribution function at contact of an equilibrium system at the same density. It arises from the Enskog's correction to the molecular chaos assumption [128]. It can be approximated for $\phi<0.6$ by [129]:

$$\chi(\phi)=\frac{1-7\phi/16-\phi^3/20}{(1-\phi)^2}. \tag{14}$$

Imposing stationarity to equation (9), we find the analytic steady-state temperature:

$$T^{\mathrm{ss}}(\phi)=\left(\frac{\epsilon(\phi)+\sqrt{\epsilon(\phi)^2+4m\Delta^2(1-\alpha^2)}}{2(1-\alpha^2)}\right)^2. \tag{15}$$

with $\epsilon(\phi)=\alpha\Delta\sqrt{\pi m}-4\gamma/\tilde{\omega}(\phi)$.

In figure 8(a), we compare this theoretical prediction with measurements performed with simulations of the effective 2D model at fixed Δ (i.e. no synchronization) and, indeed, the theory seems to work very well. This result, however, must be taken with care since the simulations reach an absorbing state at a finite packing fraction and this behavior is not predicted by the theory, which predicts zero temperature only at zero packing fraction, see the inset of figure 8(a). The assumptions of homogeneity, molecular chaos and Gaussian distribution of velocity do not hold close to or below the critical packing fraction due to the significant effect of viscous drag. As seen in figure 8(b), close to the transition, molecular chaos is broken since the velocity autocorrelation function develops a negative minimum at a time roughly equal to the mean collision time that is a clear indication of a backscattering effect. This is incompatible with the assumption of uncorrelated or Markovian collisions underlying the molecular chaos assumption. Indeed, such a theory can only predict exponentially decaying velocity autocorrelation [130–132]. This backscattering is induced by the considerable slowdown of the particles

J. Stat. Mech. (2025) 123206

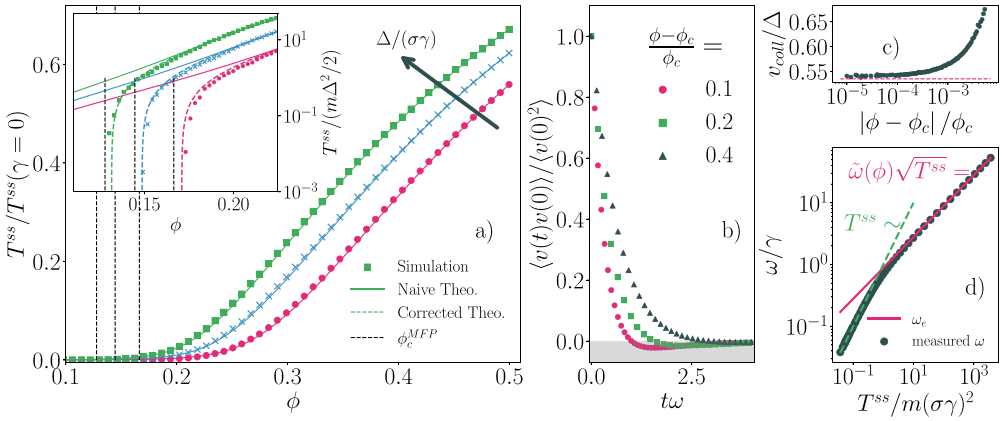

Figure 8. Comparisons between the different theories applied to the simple Δ model without synchronization and simulations. The analysis is accompanied by examples of the breakdown of the assumptions used. (a) Comparison of the theory of the simple model with the simulations. 'Naive theo.' is equation (15). 'Corrected theo.' is equations (18) and (20). The dark dashed lines are the theoretical critical packing fractions derived from the mean free path argument. The inset is in a semi-log scale close to the transition and in units of $m\Delta^2/2$. We see that when the naive theory predicts a temperature of the order $m\Delta^2/2$, the system reaches an absorbing state in simulation. $N = 5000$ and $\alpha = 0.95$. The increasing values of $\Delta/\gamma\sigma$ are: 1.25, 1.5 and 1.75. (b) Evolution of the velocity autocorrelation function as the critical density of the continuous transition is approached. The system starts to exhibit backscattering, and the prediction from the Enskog theory with molecular chaos cannot be trusted. (c) Evolution of the *pre*-colliding velocity $v_{\rm coll}$ as a function of the proximity to the absorbing state. Here, $v_{\rm coll}$ tends to saturate, implying that the active particles have a finite energy at the transition. (d) Evolution of the measured frequency of collision as the critical point is approached ($T^{\rm ss} \to 0$) by varying Δ from $\Delta_{\rm c}$, which gives a vanishing $T^{\rm ss}$ to a large value where the measured frequency of collision matches that predicted by the kinetic theory ω_e. At lower temperatures, the frequency of collision increases linearly with $T^{\rm ss}$ because it becomes proportional to the number of active particles.

before colliding with their neighbors and gaining velocities in a direction opposite to the one they came from. Treating this effect would require going beyond molecular chaos; an approach that is made possible by some tedious calculation [133]. Moreover, we observed, in figure 7, that close to the critical packing fraction, the dynamics is dominated by avalanches of active particles within a population of inactive particles. The transition could then occur via two different scenarios. Either the temperature of the active particles reaches 0 at $\phi_{\rm c}$, or their number vanishes while they still possess a finite amount of energy. The second scenario is that observed in our system, as illustrated in figure 8(c). Indeed, as the critical point is approached, the *pre*-colliding velocity v_0 (the velocity just before a collision) tends to saturate. This indicated that, at the transition, the active particles have finite energy, roughly equal to the minimal excitation possible, $m\Delta^2/2$, but their number vanishes.

This can also be inferred from the measured frequency of collision in the system as the critical point is approached. In figure 8(d), we compare the measured frequency of collision ω with that used in our theory ω_e (equation (13)). At high temperature, the measured frequency of collision ω is well approximated by the equilibrium Enskog ω_e. However, at lower energy, closer to the critical point, when the dynamics is dominated by free flight and avalanches, a large portion of the particles becomes inactive and the scaling of $\omega(\phi,T)$ changes from the equilibrium $\tilde{\omega}(\phi)\sqrt{T}$ to $\bar{\omega}(\phi)T$, with $\bar{\omega}(\phi)$being a prefactor independent of T. As discussed above, the collision frequency becomes proportional to the fraction of active particles because these particles carry finite energy and the measured temperature also scales with their fraction, leading to a linear dependence of ω with T. As a result, the ratio ω/ω_e provides a rough estimate of the fraction of active particles near the critical point.

This evidence indicates that close to the transition point, the kinetic theory breaks completely and would be hard to fix, assuming no spatial correlations in the distribution of active particles over the system. As a consequence of the significant increase in inactive particles, we adopted a more phenomenological approach that couples the population dynamics of active and inactive particles with the kinetic temperature field.

We denote P_a the probability of finding a particle in the active state, characterized by its own finite temperature T_a. The probability of being in the absorbing state is $1-P_\mathrm{a}$. We propose the following evolution equation for P_a:

$$\frac{\partial P_\mathrm{a}}{\partial t} = \frac{\omega(\phi,T_\mathrm{a})}{2} P_\mathrm{a}(1-P_\mathrm{a}) - \frac{\mathrm{e}^{-\omega(\phi,T_\mathrm{a})\tau_\mathrm{a}}}{\tau_\mathrm{a}} P_\mathrm{a}. \tag{16}$$

The first term accounts for the conversion of inactive particles to active particles due to collisions. The second term is a rate of inactivation modulated by the probability, for an active particle, of not colliding in a time τ_a, assuming that collisions are Poissonian [134]. It accounts for particles reaching the absorbing state due to an absence of collision between them and a neighbor in a time τ_a. This τ_a is acting as a cutoff with a value that will be derived below and should be inversely proportional to the drag γ. We recall that $\omega/2$ is the number of collision events per particle happening in the system per unit of time, while ω is the average frequency at which *one* particle collides with others.

To close the problem, we need to specify the temperature and the frequency of collision of the active particles. We will assume that T_a is simply given by the same equation (11) used for a homogeneous system far away from the critical region:

$$\frac{\partial T_\mathrm{a}}{\partial t} = \frac{\omega(\phi,T_\mathrm{a})}{2} \langle E' - E \rangle_{\text{active coll}} - 2\gamma T_\mathrm{a}. \tag{17}$$

Since active particles evolve in an avalanche-like manner, their neighborhood is mostly homogeneous and made of active particles. Therefore, we make the approximation that an average over collisions for active particles in the critical zone is the same as that performed in the non-critical region. In the same way, we also choose the frequency of collision between active particles to be the equilibrium one: $\omega = \omega_e$ (equation (13)). Equation (17) is thus exactly the same as equation (11). We now understand that the temperature prediction from the naive theory was correct, but only as a description

J. Stat. Mech. (2025) 123206

of a subset of the system: the active particles, for which the equilibrium frequency of collision is a good approximation. We immediately obtain the temperature of the whole system:

$$T_{\mathrm{a}}^{\mathrm{ss}} = \left(\frac{\epsilon + \sqrt{\epsilon^2 + 4m\Delta^2 (1-\alpha^2)}}{2(1-\alpha^2)} \right)^2 \qquad (18)$$
$$T^{\mathrm{ss}} = P_{\mathrm{a}}^{\mathrm{ss}} T_{\mathrm{a}}^{\mathrm{ss}}.$$

Far away from the critical point, $P_{\mathrm{a}}^{\mathrm{ss}} \to 1$ and equation (15) is recovered. Moreover, as argued above, at the critical point, $T_{\mathrm{a}}^{\mathrm{ss}}$ is finite, and the criticality is provided solely by the fraction of active particles going to 0 and not by the activity of the active particles.

With these assumptions, since T_{a} is decoupled from P_{a} and varies slowly close to the transition, we can assume it as a constant around the critical point. Hence equation (16) reads:

$$\tau_{\mathrm{a}} \frac{\partial P_{\mathrm{a}}(t)}{\partial t} = \left(\frac{\tau_{\mathrm{a}}\omega_e}{2} - \mathrm{e}^{-\tau_{\mathrm{a}}\omega_e} \right) P_{\mathrm{a}} - \frac{\tau_{\mathrm{a}}\omega_e}{2} P_{\mathrm{a}}^2, \qquad (19)$$

and this has the following stable non-negative stationary solution:

$$P_a^{\mathrm{ss}} = \begin{cases} \dfrac{\tau_{\mathrm{a}}\omega_e(\phi, T_{\mathrm{a}}^{\mathrm{ss}}) - 2\mathrm{e}^{-\tau_{\mathrm{a}}\omega_e(\phi, T_{\mathrm{a}}^{\mathrm{ss}})}}{\tau_{\mathrm{a}}\omega_e(\phi, T_{\mathrm{a}}^{\mathrm{ss}})} & \text{if } \tau_{\mathrm{a}}\omega_e > W_0(2) \\ 0 & \text{else,} \end{cases} \qquad (20)$$

with W_0 being the principal branch of the Lambert W function.Here, $P_{\mathrm{a}}^{\mathrm{ss}}$ varies continuously, and the transition happens when the mean free time $1/\omega_e$ of the active particle is of the same order ($W_0(2) \simeq 0.85$) as the stopping time τ_{a}. It is gratifying to observe that equation (19) is the mean-field equation describing the conserved directed percolation universality class, which is the correct equation to describe the vicinity of our phase transition [116]. At this point, it is interesting to make a parallel with models on a lattice. As said before, the criticality in our model comes from the vanishing of P_{a} while the temperature of the active particles is fixed. This behavior closely resembles lattice models in the conserved directed percolation universality class, where the order parameter is the number of active particles and for which the activity kick allowing a particle to move on the lattice is fixed and finite [109, 135].

To close our equations, we must determine a suitable value for τ_{a}. This can be achieved, for example, by finding an independent prediction for ϕ_{c}. An argument presented in [95] allows us to find a lower bound for the critical packing fraction of the continuous transition. If we assume spatial homogeneity, at the critical packing fraction, particles must collide on average with zero velocity. Below this density, particles do not have sufficient momentum after a collision to reach their neighbors, which ultimately leads to the system reaching an absorbing state. Hence, after a collision, two particles will simply have a velocity Δ which, on average, is dissipated to zero over a distance

J. Stat. Mech. (2025) 123206

Δ/γ. This distance must be equal to the mean free path, which lets us derive the equation of the critical packing fraction:

$$l(\phi_c) = \Delta/\gamma, \tag{21}$$

with $l(\phi)$being the mean free path. Surprisingly, this simple reasoning, whose results are presented as a dashed vertical bar in the inset of figure 8, predicts a critical packing fraction in good agreement with the simulations. Note that with this argument, it is assumed that the system transitions to the absorbing state uniformly, and that the pre-collisional velocity, $v_{\rm coll}$, vanishes at the transition point. This assumption would suggest $T_a(\phi_c) = 0$, which is not consistent with the way the transition occurs in the simulations.

We can inject this critical packing fraction into our theory. We expect the transition to happen when $\tau_a\omega_e(\phi_c, T_a) = W_0(2)$. Using the Gaussian relation, $\omega_e = \sqrt{\pi T_a(\phi)/(2m)}/l(\phi)$ and supposing that T_a is of the order $m\Delta^2/2$ at the transition, we finally obtain an expression for τ_a from the mean free path argument:

$$\tau_a^{\rm MFP} = \frac{2W_0(2)}{\sqrt{\pi}}\frac{1}{\gamma}. \tag{22}$$

As expected, τ_a is proportional to $1/\gamma$. Our equations are now devoid of adjustable parameters. In the inset of figure 8(a), we compare this new theory (equations (18), (20) and (22)) with the simulations. The agreement is very satisfactory, especially in view of the assumption made (Gaussianity of the active particles, homogeneity, absence of spatial and temporal correlation, mean-field approach, etc). The temperatures in the inset are rescaled by $m\Delta^2/2$ to emphasize the fact that the system reaches an absorbing state when the energy of the active particles is close to the minimal excitation $m\Delta^2/2$. Indeed, the corrected theory predicts the transition when the naive theory—now representing the theoretical energy of the active particles only—is close to $m\Delta^2/2$. Three points, however, warrant attention. (i) The equations are solved in the mean-field approximation; hence they cannot be exactly close to the transition and this would be reflected, for example, in the discrepancy of critical exponents. (ii) With the new theory, the transition is not predicted to happen exactly at the critical packing fraction obtained from the mean free path argument $\phi_c^{\rm MFP}$, even if it is used to find τ_a. This is because the temperature of the active particle predicted equation (18) at $\phi_c^{\rm MFP}$ is obviously not strictly equal to $m\Delta^2/2$. (iii) The coefficient of restitution α is close to 1; hence, the probability distribution is expected to be almost Gaussian in the active region where the drag is not playing a major role [136, 137]. The predictions would thus not be as good for systems with stronger dissipation at collision.

4.2. Synchronization-dependent Δ model

Here, we extend the theory outlined in the previous section to incorporate synchronization. At first, we assume that the discontinuous transition occurs far away from the

J. Stat. Mech. (2025) 123206

zone where the continuous transition occurs, thus neglecting the inactivation dynamics described by the population dynamics equation (16) and effectively setting $P_\mathrm{a} = 1$, which implies $T = T_\mathrm{a}$.

The model equation (7) implies that the value of Δ_{ij} depends on the time since the last collision for both particles involved, i and j. If at least one particle has traveled for a time smaller than τ_s, the value of Δ_{ij} is Δ, otherwise it is set to 0. In this case, an exact calculation of the collisional average in equation (11) is challenging; however, we can make a reasonable estimation by assuming that the synchronization-dependent Δ_{ij} can be replaced by an effective one: $\overline{\Delta}$. Here, we propose:

$$\overline{\Delta}\left(\phi, T_\mathrm{a}, \tau_\mathrm{s}\right) \equiv \overline{\Delta}_{ij} = \Delta\left(1 - \mathrm{e}^{-2\omega_e(\phi, T_\mathrm{a})\tau_\mathrm{s}}\right) \tag{23}$$

where the term in parentheses represents the probability that at least one of the two particles involved in the collision has collided at a time smaller than τ_s in the past, again assuming uncorrelated particles, Poissonian collisions and an equilibrium frequency of collision. With this effective $\bar{\Delta}$, it becomes evident that the synchronization mechanism results from the competition between the collision frequency ω and the synchronization rate $1/\tau_\mathrm{s}$. At low frequencies of collision compared to the synchronization rate, $\overline{\Delta}$ is small, while the opposite is true for high values of $\omega\tau_\mathrm{s}$.

One final assumption is needed. We simplify the averages over collisions which include a Δ_{ij} by performing the following approximation when calculating the average of an arbitrary function $h(\boldsymbol{v}_i, \boldsymbol{v}_j)$:

$$\left\langle h\left(\boldsymbol{v}_i, \boldsymbol{v}_j\right) \Delta_{ij} \right\rangle_\mathrm{coll} \simeq \left\langle h\left(\boldsymbol{v}_i, \boldsymbol{v}_j\right) \right\rangle_\mathrm{coll} \overline{\Delta}. \tag{24}$$

This approximation essentially neglects any correlations between particle velocities and their synchronization state.

This simplification allows us to derive an analytical expression for $G(\phi, T_\mathrm{a}, \tau_\mathrm{s})$:

$$G\left(\phi, T_\mathrm{a}, \tau_\mathrm{s}\right) = \frac{\omega}{2}\left(m\overline{\Delta}^2 + \alpha\overline{\Delta}\sqrt{\pi m T_\mathrm{a}} - T_\mathrm{a}\left(1 - \alpha^2\right)\right) - 2\gamma T_\mathrm{a}, \tag{25}$$

which has the same form as that found for the simple Δ model without synchronization, except that Δ is replaced by the effective $\overline{\Delta}$, which depends on the packing fraction, temperature and synchronization time. This effective Δ radically changes the energy landscape of the transition compared to the continuous one. To see this, it is useful to define an effective non-equilibrium thermodynamic potential:

$$U\left(T_\mathrm{a}, \phi, \tau_\mathrm{s}\right) = -\int_0^{T_\mathrm{a}} G\left(T_\mathrm{a}', \phi, \tau_\mathrm{s}\right) \mathrm{d}T_\mathrm{a}', \tag{26}$$

such that equation (9) can be rewritten as a gradient descent:

$$\frac{\partial T_\mathrm{a}}{\partial t} = -\frac{\partial U}{\partial T_\mathrm{a}}, \tag{27}$$

J. Stat. Mech. (2025) 123206

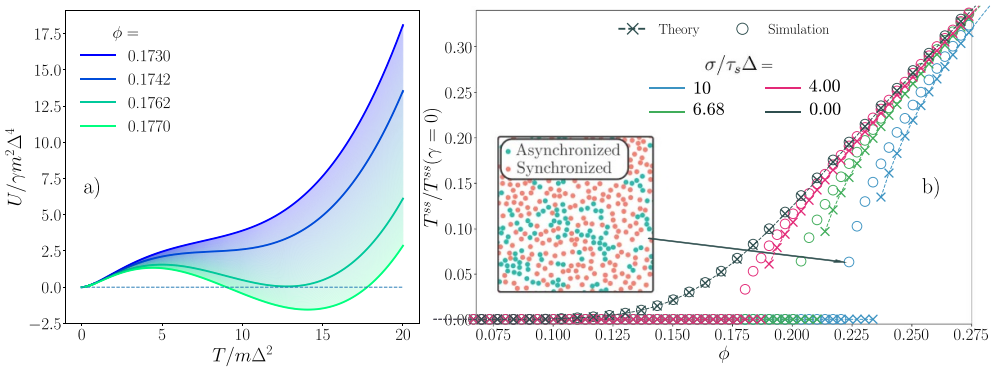

Figure 9. (a) The theoretical non-equilibrium potential U as a function of T for different ϕ and $1/(\gamma\tau_s) = 10$, $\Delta/(\gamma\sigma) = 2.5$ and $\alpha = 0.95$. The potentials behave exactly as an equilibrium potential for a thermodynamic first-order phase transition as the order parameter is changed. (b) The effect of synchronization over the nature of transition and the critical packing fraction: $N = 20\,000$, $\Delta/(\gamma\sigma) = 2.5$ and $\alpha = 0.95$. The inset is a typical snapshot of the system close to the transition point.

and stable steady states are hence given by local minima of the effective non-equilibrium potential.

As a qualitative check, when $1/\tau_s > 0$, the non-equilibrium potential given by the integral of equation (25) has the same functional shape as an equilibrium Landau free energy [138, 139] of a system undergoing a first-order phase transition, as seen in figure 9(a). A quantitative comparison between the simulation and the theory is depicted in figure 9(b). The theory, corresponding to the local minima of U or, equivalently, the root of G (found numerically), consistently predicts the observed transition. We note that the mean-field nature of the solution limits our ability to accurately determine the critical packing fraction. Near the transition point, density and spatial synchronization inhomogeneities arise due to the local nature of synchronization and due to the dissipative nature of the collisions between synchronized particles, as depicted in the snapshot in the inset of figure 9(b) and in figure 7. We can see clusters of synchronized and asynchronized particles, which can reasonably explain the inaccuracies of the theories (especially close to the transition) together with the effective Δ approximation.

It is interesting to further explore the similarities between our effective potential and the Landau free energy of an equilibrium system. This resemblance is, for example, highlighted by the Taylor expansion of the non-equilibrium potential:

$$U = \gamma T_a^2 - \frac{\tilde{\omega}}{5}\left[2\tilde{\omega}\tau_s\Delta\left(\sqrt{\pi m}\alpha + 2m\tilde{\omega}\tau_s\Delta\right) - \left(1-\alpha^2\right)\right]T_a^{5/2} + \sum_{n=6}^{\infty}(-1)^n K_{n/2}T_a^{n/2}, \quad (28)$$

where $K_{n/2}$ are positive numbers for $n \geqslant 6$ [54, 140–143].

For infinite system sizes, the stability of the phases and their robustness to small perturbations are controlled by the depths of the minima corresponding to these phases.

Specifically, for small damping γ, the stability of the absorbing state with respect to small perturbations is dictated by the sign of $K_{5/2}$:

$$K_{5/2} = \tilde{\omega}\left(2\tilde{\omega}\tau_{\mathrm{s}}\Delta\left(\sqrt{\pi m}\alpha + 2m\tilde{\omega}\tau_{\mathrm{s}}\Delta\right) - \left(1-\alpha^2\right)\right)/5, \tag{29}$$

playing a role similar to the ϵ of [33]. When $K_{5/2} < 0$, the dissipation exceeds the energy injection, leading to an easily unstable absorbing state with respect to small perturbations. Conversely, when $K_{5/2} > 0$, the absorbing state is stable. We conclude that the critical packing fraction ϕ_{c} approximately satisfies $K_{5/2}(\phi_{\mathrm{c}}) = 0$ when the drag can be neglected. Importantly, we see that for this transition, the critical packing fraction is approximately given by a competition between the average energy injected and dissipated at collision. Instead, for the continuous transition, the critical packing fraction was dictated by the competition between energy injection at collision and dissipation during the free flight. Notably, the mean free path argument (equation (21)) predicts a critical packing fraction for the continuous transition independent of α. This is consistent with our understanding that synchronization allows the system to reach the absorbing state for a range of packing fractions that would have corresponded to the active phase in the asynchronized case. Increasing ϕ, and in turn the collision rate $\omega(T,\phi)$, gives the grains less time to synchronize between collisions, which happens over a characteristic time τ_{s}. For the effective 2D model, we have numerically confirmed that the typical time between collisions $1/\omega$ is always of the same order as (but slightly below) τ_{s} in the first active state after the discontinuous transition [1, 144–147]:

$$\frac{\partial T_{\mathrm{a}}}{\partial t} = -\frac{\partial U}{\partial T_{\mathrm{a}}} + \sqrt{2KT_{\mathrm{a}}}\eta(t)\,. \tag{30}$$

[148–151].

Thus far, in our theoretical model with synchronization, we have neglected the possible presence of inactive particles by setting $P_{\mathrm{a}} = 1$, effectively limiting ourselves to cases where $T_{\mathrm{a}}(\phi_{\mathrm{c}}^{+}) \gg m\Delta^2/2$. In these cases, any finite synchronization time would lead to a discontinuous transition; however, in cases where our theory with $P_{\mathrm{a}} = 1$ predicts a discontinuous transition with a theoretical ϕ_{c}, such that $T_{\mathrm{a}}(\phi_{\mathrm{c}}^{+}) < m\Delta^2/2$, the expected observed transition is in fact continuous. This is because, in these cases, as the density is decreased, the population of inactive particles would begin to grow due to the drag, eventually leading the system to an absorbing state before the dissipative collisions can provoke the theoretically predicted discontinuous phase transition. To correctly account for this effect, we simply need to restore, in the theory, the evolution equation for the proportion of active particles instead of assuming $P_{\mathrm{a}} = 1$.

This situation occurs, for example, when τ_{s} is very large, as particles cannot synchronize before coming to a complete stop. Indeed, the synchronization timescale is not competing against the diverging timescale linked to the criticality of the continuous transition but against the mean collision time of the active particles, which is finite. Hence, while the population of inactive particles may synchronize, the active particle population does not and the transition follows the same route as without synchronization. We provide more details in appendix D.

J. Stat. Mech. (2025) 123206

Finally, we note that the theoretical treatment of the model with synchronization could have been approached by introducing an additional dynamical variable: the fraction of synchronized particles, instead of relying on an effective Δ. This method, analogous to the population dynamics introduced for the active/inactive populations of particles near the continuous transition, offers slightly better results compared to the effective Δ approach, albeit at the expense of a less clear physical picture and a more complex theoretical treatment since the description of the system would then require at least three fields: the temperature of the active particles, the fraction of active particles and the fraction of synchronized particles.

5. Hydrodynamics of the active state

We now derive the hydrodynamic theory of the effective 2D model in its active state. In doing so, we will neglect synchronization effects and any heterogeneity in the population of active particles. This approach allows us to quantitatively predict the structural properties of the active states.

5.1. Derivation of the hydrodynamics of the model

Up to this point, the theory we use is neglecting all spatial dependence. Starting from the Boltzmann equation of our system and the single-particle microscopic velocity and position distribution, we can derive the corresponding hydrodynamical equations through its velocity moments [152–154]. Following [136, 155], the Boltzmann equation dictating the evolution of the one particle distribution function $f(\boldsymbol{r},\boldsymbol{v},t)$ in our system is given by:

$$\frac{\partial f\left(\boldsymbol{r},\boldsymbol{v},t\right)}{\partial t}+\boldsymbol{v}\cdot\frac{\partial f}{\partial \boldsymbol{r}}-\gamma\frac{\partial}{\partial \boldsymbol{v}}\cdot\left(\boldsymbol{v}f\right)=J\left(\boldsymbol{r},\boldsymbol{v}|f,f\right), \tag{31}$$

where J is the collision kernel:

$$\begin{aligned} J\left(\boldsymbol{r}_i,\boldsymbol{v}_i|f,f\right)=\chi\sigma_{ij}\int \mathrm{d}\boldsymbol{v}_j\int \mathrm{d}\hat{\boldsymbol{\sigma}}_{ij}\big[&\Theta\left(-\boldsymbol{v}_{ij}\cdot\hat{\boldsymbol{\sigma}}_{ij}+2\Delta_{ij}\right)\left(-\boldsymbol{v}_{ij}\cdot\hat{\boldsymbol{\sigma}}_{ij}+2\Delta_{ij}\right)\\ &\times\frac{f\left(\boldsymbol{r}_j,\boldsymbol{v}_j''\right)f\left(\boldsymbol{r}_i+\boldsymbol{\sigma}_{ij},\boldsymbol{v}_i''\right)}{\alpha^2}\\ &-\Theta\left(-\boldsymbol{v}_{ij}\cdot\hat{\boldsymbol{\sigma}}_{ij}\right)\left(-\boldsymbol{v}_{ij}\cdot\hat{\boldsymbol{\sigma}}_{ij}\right)f\left(\boldsymbol{r}_j,\boldsymbol{v}_j\right)f\left(\boldsymbol{r}_i+\boldsymbol{\sigma}_{ij},\boldsymbol{v}_i\right)\Big]. \end{aligned} \tag{32}$$

Additionally, $\boldsymbol{v}_i''$ and $\boldsymbol{v}_j''$ are the pre-collisional velocities that would lead to the post-collisional velocities $\boldsymbol{v}_i$ and $\boldsymbol{v}_j$. By inverting equation (5), we find:

$$\begin{aligned} \boldsymbol{v}_i''&=\boldsymbol{v}_i+\frac{1+\alpha^{-1}}{2}\left(\boldsymbol{v}_{ij}\cdot\hat{\boldsymbol{\sigma}}_{ij}\right)\hat{\boldsymbol{\sigma}}_{ij}-\Delta_{ij}\alpha^{-1}\hat{\boldsymbol{\sigma}}_{ij},\\ \boldsymbol{v}_j''&=\boldsymbol{v}_j-\frac{1+\alpha^{-1}}{2}\left(\boldsymbol{v}_{ij}\cdot\hat{\boldsymbol{\sigma}}_{ij}\right)\hat{\boldsymbol{\sigma}}_{ij}+\Delta_{ij}\alpha^{-1}\hat{\boldsymbol{\sigma}}_{ij}. \end{aligned} \tag{33}$$

J. Stat. Mech. (2025) 123206

Molecular chaos was again assumed in equation (32) to close the equation for the single velocity distribution. The collisional contribution J takes the usual form of a master equation [156]. While the first term accounts for collisions increasing the number of particles with velocity $\boldsymbol{v}_i$, the second term is a loss term for $\boldsymbol{v}_i$ due to collisions. Both terms are modulated by the relative velocities of the particles along the collision since faster particles collide more often. Here, Θ is the Heaviside function, ensuring that collisions are physical and particles are headed toward each other before colliding. Finally, the factor $1/\alpha^2$ comes from the Jacobian associated with the change in variable $\boldsymbol{v}'' \to \boldsymbol{v}$ and the change in normal velocity at collision [156].

The macroscopic hydrodynamic (mass) density ρ, velocity $\boldsymbol{u}$ and temperature T fields can be defined through the moment of the single particle distribution:

$$\begin{aligned}
\rho(\boldsymbol{r},t) &= m\int \mathrm{d}\boldsymbol{v} f(\boldsymbol{r},\boldsymbol{v},t),\\
\rho(\boldsymbol{r},t)\,\boldsymbol{u}(\boldsymbol{r},t) &= m\int \mathrm{d}\boldsymbol{v}\boldsymbol{v} f(\boldsymbol{r},\boldsymbol{v},t),\\
\rho(\boldsymbol{r},t)\,T(\boldsymbol{r},t) &= m\int \mathrm{d}\boldsymbol{v}\left(\boldsymbol{v}-\boldsymbol{u}(\boldsymbol{r},t)\right)^2 f(\boldsymbol{r},\boldsymbol{v},t).
\end{aligned} \tag{34}$$

We also define the number density n and packing fraction field ϕ; useful quantities related to the (mass) density through $\rho(\boldsymbol{r},t) = mn(\boldsymbol{r},t) = 4m\phi(\boldsymbol{r},t)/\pi\sigma^2$. By multiplying the Boltzmann equation (equation (31)) with different powers of v or $u - v$, the evolution equations for the hydrodynamical fields can be obtained. Assuming, at first, a constant Δ (no synchronization), we obtain:

$$\begin{aligned}
\frac{\partial\rho}{\partial t} + \boldsymbol{u}\cdot\boldsymbol{\nabla}\rho &= -\rho\boldsymbol{\nabla}\cdot\boldsymbol{u},\\
\frac{\partial\boldsymbol{u}}{\partial t} + \boldsymbol{u}\cdot\boldsymbol{\nabla}\boldsymbol{u} &= -\rho^{-1}\boldsymbol{\nabla}\cdot\boldsymbol{\Pi} - \gamma\boldsymbol{u},\\
\frac{\partial T}{\partial t} + \boldsymbol{u}\cdot\boldsymbol{\nabla}T &= -n^{-1}\left[\boldsymbol{\nabla}\cdot\boldsymbol{q} + \boldsymbol{\Pi}:(\boldsymbol{\nabla}\boldsymbol{u})\right] + \tilde{G}(\boldsymbol{r},t),
\end{aligned} \tag{35}$$

where some dependencies on $\boldsymbol{r}$ and t have been omitted for ease of reading. Now that the microscopic velocity has been integrated, we will simply denote $\boldsymbol{\nabla}$ as the spatial gradient. Here, ':' is the dyadic dot product understood as $(\boldsymbol{A}:\boldsymbol{B}) = \sum_{i,j} A_{ij}B_{ij}$, while $\boldsymbol{\Pi}$ and $\boldsymbol{q}$ are, respectively, the *microscopic* stress tensors and the *microscopic* heat flux.

Equations (35) are currently undetermined since the currents and G are defined from averages with respect to the microscopic probability distribution. To obtain a useful hydrodynamic description, we must assume or derive a closure to relate the currents to the macroscopic fields. One widely used approach to approximate the velocity distribution involves expanding it in terms of the gradient of the hydrodynamical fields, a method commonly known as the Chapman–Enskog expansion [136, 157–160]. The important assumption is that the spatial and temporal dependence of the distribution of velocity at a given point can be solely described by a functional dependence

J. Stat. Mech. (2025) 123206

on the hydrodynamic fields [161]: $f(\boldsymbol{r},\boldsymbol{v},t) \equiv f[\boldsymbol{v}|\rho(\boldsymbol{r},t),\boldsymbol{u}(\boldsymbol{r},t),T(\boldsymbol{r},t)]$. The Boltzmann equation is then solved perturbatively, order by order, using the following expansion:

$$\begin{aligned} \boldsymbol{\nabla} &\to \varepsilon \boldsymbol{\nabla} \\ f &= f^{(0)} + \varepsilon f^{(1)} + \dots \end{aligned} \tag{36}$$

Here, ε is a dummy expansion parameter keeping track of the order of the gradient for the velocity distribution and set to 1 at the end of the procedure. The solutions are expected to be valid only for an almost homogeneous system with weak contributions coming from the gradients.

Performing the Chapman–Enskog expansion in the first order leads to the following constitutive relations [136]:

$$\begin{aligned} \boldsymbol{\Pi} &= p\mathbf{1} + \eta\left(\boldsymbol{\nabla}\boldsymbol{u} + (\boldsymbol{\nabla}\boldsymbol{u})^T - (\boldsymbol{\nabla}\cdot\boldsymbol{u})\,\mathbf{1}\right) + \zeta\,(\boldsymbol{\nabla}\cdot\boldsymbol{u})\,\mathbf{1} \\ \boldsymbol{q} &= -\kappa\boldsymbol{\nabla}T - \mu\boldsymbol{\nabla}n \\ \tilde{G} &= G + \nu\boldsymbol{\nabla}\cdot\boldsymbol{u}, \end{aligned} \tag{37}$$

where $\mathbf{1}$ is the unit tensor, p is the hydrostatic pressure, η and ζ are, respectively, the shear and bulk viscosity, and κ and μ are the thermal and diffusive heat conductivity. The latter is 0 at equilibrium and arises in our model from the coupling between the density gradient and temperature through the inelastic nature of the collisions [162]. Here, $G \equiv G(\rho(\boldsymbol{r},t),T(\boldsymbol{r},t))$ has the same functional shape as equation (12), while ν is an additional non-equilibrium transport coefficient [125]. Other transport coefficients technically arise for $\tilde{G}$ at the hydrodynamic order k^2 in the hydrodynamic equations. However, these are omitted here as their contributions are negligible.

Given the typical smallness of the correction due to the presence of a Δ or γ [136, 163] over a wide range of values, we will use the equilibrium hard disk transport coefficients in what follows. We provide additional details on the chosen expressions for all the numerical values of these transport coefficients in appendix E.

5.2. Hydrodynamic matrix and stability analysis

Equations (37), together with the constitutive relations equations (35), are non-linear and difficult to analyze. However, their linearization with respect to the homogeneous solution found in section 4 still provides useful information, notably concerning the stability of this reference homogeneous state.

We expand the density, velocity and temperature field around the homogeneous steady state $(\rho,\boldsymbol{u},T) = (\rho_0,0,T_0)$:

$$\begin{aligned} \rho(\boldsymbol{r},t) &= \rho_0 + \delta\rho(\boldsymbol{r},t) \\ \boldsymbol{u}(\boldsymbol{r},t) &= 0 + \delta\boldsymbol{u}(\boldsymbol{r},t) \\ T(\boldsymbol{r},t) &= T_0 + \delta T(\boldsymbol{r},t) \end{aligned} \quad . \tag{38}$$

J. Stat. Mech. (2025) 123206

Here, ρ_0 corresponds to the global density imposed in the system, and T_0 is given by the solution of the homogeneous equation introduced in section 4: $G(\phi_0, T_0 \equiv T^{\text{ss}}) = 0$ (equation (15) without synchronization, and equation (27) with synchronization).

Following [94, 164], we perform a Fourier transform, with k being the momentum variable, and we define the longitudinal $\delta u_{\parallel}(\boldsymbol{k},t) = \hat{\boldsymbol{k}} \cdot \delta \boldsymbol{u}(\boldsymbol{k},t)$ and transversal velocity field $\delta u_{\parallel}(\boldsymbol{k},t) = \hat{\boldsymbol{k}}_{\perp} \cdot \delta \boldsymbol{u}(\boldsymbol{k},t)$, with $\hat{\boldsymbol{k}}$ and $\hat{\boldsymbol{k}}_{\perp}$being the unit vector in the direction of $\boldsymbol{k}$ and perpendicular to $\boldsymbol{k}$, respectively. We define $\boldsymbol{\Psi}(\boldsymbol{k},t) = (\delta\rho, \delta u_{\parallel}, \delta u_{\perp}, \delta T)$, a vector containing the linearized hydrodynamic field. In the first order, equations (35) then read:

$$\frac{\partial \boldsymbol{\Psi}(\boldsymbol{k},t)}{\partial t} = \boldsymbol{M}(|\boldsymbol{k}|)\,\boldsymbol{\Psi}(\boldsymbol{k},t), \tag{39}$$

with $\boldsymbol{M}(|\boldsymbol{k}|)$being the so-called hydrodynamical matrix:

$$\boldsymbol{M}(k) = \begin{pmatrix} 0 & -\mathrm{i}\rho_0 k & 0 & 0 \\ -\mathrm{i}k\dfrac{p_\rho|_{\rho_0,T_0}}{\rho_0} & -\gamma - \dfrac{\eta_0^{\parallel}}{\rho_0}k^2 & 0 & -\mathrm{i}k\dfrac{p_T|_{\rho_0,T_0}}{\rho_0} \\ 0 & 0 & -\gamma - \dfrac{\eta_0^{\perp}}{\rho_0}k^2 & 0 \\ G_\rho|_{\rho_0,T_0} - \dfrac{\mu_0}{n_0}k^2 & -\mathrm{i}k\dfrac{p_0+\nu_0}{n_0} & 0 & G_T|_{\rho_0,T_0} - \dfrac{\kappa_0}{n_0}k^2 \end{pmatrix}. \tag{40}$$

The subscript 0 on the pressure and each transport coefficient indicates their evaluation in the homogeneous state. For conciseness, the derivatives are denoted by a subscript: $\partial F/\partial X \equiv F_X$. Here, $\eta_0^{\parallel} = \eta_0 + \zeta_0$ is the longitudinal viscosity and $\eta_0^{\perp} = \eta_0$ is the transverse viscosity. As usual, the transverse velocity field decouples from the other modes in the linear order. The results obtained are consistent with related results found in the granular system literature [94, 156, 165, 166], and correctly reduce to equilibrium hydrodynamics in the absence of energy change ($G = 0$) and damping [164].

From equation (39), it is clear that to the first order, the time evolution of the perturbation around the steady state is characterized by a sum of exponentials with exponents corresponding to the eigenvalues $z(k)$ of $\boldsymbol{M}(k)$. Indeed, the evolution of the hydrodynamic fields can be expressed as:

$$\boldsymbol{\Psi}(t) = \mathrm{e}^{Mt}\boldsymbol{\Psi}(0) = \sum_{\lambda} \mathrm{e}^{z_\lambda t}\boldsymbol{\psi}_\lambda(\boldsymbol{\varphi}_\lambda \cdot \boldsymbol{\Psi}(0)), \tag{41}$$

where $\boldsymbol{\varphi}_\lambda$ and $\boldsymbol{\psi}_\lambda$ are the left and right normalized eigenvectors corresponding to the λth eigenvalue, respectively, and we used the completeness relation $\sum_\lambda \boldsymbol{\psi}_\lambda \boldsymbol{\varphi}_\lambda^T = \mathbf{1}$.

From equation (41), we understand that the stability of the homogeneous state is related to the negativity of the real part of the eigenvalues of $\boldsymbol{M}$. An analysis of the positivity of the eigenvalues utilizing the Routh–Hurwitz stability criterion [167] demonstrates, as in previous studies of related systems [94], that the active state is stable. Consequently, we conclude that the homogeneous state predicted by the kinetic theory in section 4 remains stable against spatial inhomogeneity.

J. Stat. Mech. (2025) 123206

This means that the hydrodynamic theory, which goes beyond the mean-field approach, also fails to predict a phase transition since the non-zero homogeneous state is always stable, even at low ϕ. This justifies, *a posteriori*, the introduction of an inactive particle population in the kinetic theory of section 4 in order to achieve a continuous transition.

5.3. Hydrodynamic modes, dynamic and static correlation functions

The eigenvalues of the hydrodynamic matrix are interesting because they inform us about the process in operation, on different length scales, in our system. In figure 10(a), we numerically computed the eigenvalues of $\boldsymbol{M}$ for typical values of γ and Δ. We omitted the eigenvalue related to the transverse velocity field since it is trivial. The imaginary part of z corresponds to propagating waves, while the real part corresponds to damped or diffusive excitations. We see that only at intermediate values of k, in region II, propagating waves are present. Notably, in the inset, we provide a zoom-in on region I, where it is clear that at very low wavenumber, there is a regime without propagating waves. We also observe that only one eigenvalue vanishes at $k=0$ while the others do not. This is directly related to the fact that only the density is conserved in this system.

While the direct measurement of the evolution of hydrodynamic modes is challenging both experimentally and numerically, spatio-temporal correlations of fluctuations are more accessible [164]. We define the correlation functions we will employ as follows (with a slight abuse of notation):

$$\begin{aligned}
\boldsymbol{F}_{ab}(\boldsymbol{k},t) &\equiv \lim_{t'\to\infty}\left\langle \boldsymbol{\Psi}_{\mathrm{a}}(\boldsymbol{k},t')\,\boldsymbol{\Psi}_{b}^{T}(-\boldsymbol{k},t'+t)\right\rangle \\
&\equiv \lim_{t'\to\infty}\left\langle \delta a(\boldsymbol{k},t')\,\delta b(-\boldsymbol{k},t'+t)\right\rangle \\
\boldsymbol{S}_{ab}(\boldsymbol{k}) &\equiv \boldsymbol{F}_{ab}(\boldsymbol{k},0) \\
\boldsymbol{S}_{ab}(\boldsymbol{k},w) &\equiv \int_{-\infty}^{\infty} \mathrm{d}t \mathrm{e}^{-\mathrm{i}wt}\boldsymbol{F}_{ab}(\boldsymbol{k},|t|)\,,
\end{aligned} \tag{42}$$

where a and b are hydrodynamic fields. If a and b are the density ρ (or n up to a mass factor), the correlation functions defined above will be called, respectively, the intermediate scattering function, the structure factor and the dynamic structure factor. Note that here the subscripts correspond to the element of the matrix and not to the derivative.

To perform the averages $\langle\cdot\rangle$ over different steady-state realizations, we need to either introduce a probability distribution for the steady-state values of the fields or a dynamical noise to the hydrodynamic equations, equation (39). We chose the latter approach. When the steady state reached by the hydrodynamical fields is an equilibrium one, the probability distribution of the noises for the linearized equations, assuming Gaussianity, is equivalently found using the Mori–Zwanzig projection method [168], Einstein's fluctuation theory or via the fluctuation dissipation theorem [169–171]. Out of equilibrium, the choice of an appropriate probability distribution remains ambiguous and, in principle, must be derived from the microscopic dynamics [172–179]. However, in our work,

J. Stat. Mech. (2025) 123206

we will simply assume that the noise has the same form as in equilibrium, a hypothesis often used with success in granular systems [128, 180]. Therefore, the fluctuating hydrodynamic equations take the form:

$$\frac{\partial \boldsymbol{\Psi}(\boldsymbol{k},t)}{\partial t} = \boldsymbol{M}(|\boldsymbol{k}|)\,\boldsymbol{\Psi}(\boldsymbol{k},t) + \boldsymbol{\Xi}(\boldsymbol{k},t)\,, \tag{43}$$

where $\boldsymbol{\Xi}$ is a Gaussian process with the following statistics:

$$\begin{aligned} \langle \boldsymbol{\Xi}(\boldsymbol{k},t)\rangle &= 0, \\ \langle \boldsymbol{\Xi}(\boldsymbol{k},t)\,\boldsymbol{\Xi}^{T}(\boldsymbol{k}',t')\rangle &\equiv (2\pi)^2\,\boldsymbol{C}(\boldsymbol{k})\,\delta(t-t')\,\delta(\boldsymbol{k}+\boldsymbol{k}')\,, \end{aligned} \tag{44}$$

with

$$\boldsymbol{C}(\boldsymbol{k}) = 2\boldsymbol{k}^2 T_0 \begin{pmatrix} 0 & 0 & 0 & 0 \\ 0 & \eta_0^{\parallel}/\rho_0^2 & 0 & 0 \\ 0 & 0 & \eta_0^{\perp}/\rho_0^2 & 0 \\ 0 & 0 & 0 & \kappa_0 T_0/n_0^2 \end{pmatrix}. \tag{45}$$

The dependence on $\boldsymbol{k}^2$ of the correlation $\boldsymbol{C}$ ensures local conservation of momentum and energy by the noise. At equilibrium, this dependence is necessary because hydrodynamic fields must be locally conserved, implying that noises must be a divergence of a random current. In this non-equilibrium context, where neither momentum nor temperature are conserved, this requirement is less immediate. Nevertheless, the source of stochasticity remains the discrete collisions that the particles making up the fluid undergo, which do conserve momentum. The temperature field is, however, not conserved by collisions, and a term in k^0 is therefore expected. However, such a term is usually found to be proportional to the non-Gaussianity of the velocity distribution [176], which we found to be negligible. Finally, we note that in the linear regime, the noises are non-multiplicative since their coefficients are evaluated at the homogeneous field values.

With a way to perform averages, we can now compute the correlation functions. From equation (41), it is clear that the intermediate scattering function is a sum of exponentials, which implies that the dynamic structure factor is a sum of Lorentzian, one for each hydrodynamic mode entering into the correlation function. Since equation (43) is a generalized Ornstein–Uhlenbeck process, we can immediately obtain $\boldsymbol{S}(\boldsymbol{k},w)$ from a time Fourier transform of equation (43) and the Wiener–Khintchine–Einstein theorem:

$$\boldsymbol{S}(\boldsymbol{k},w) = \left(\boldsymbol{M}(\boldsymbol{k}) - \mathrm{i}w\mathbf{1}\right)^{-1} \boldsymbol{C}(\boldsymbol{k}) \left(\boldsymbol{M}^{T}(-\boldsymbol{k}) + \mathrm{i}w\mathbf{1}\right)^{-1}. \tag{46}$$

It can be integrated to obtain the static correlation function $\boldsymbol{S}(\boldsymbol{k})$. However, it is usually easier to derive it from the equal-time relation [131]:

$$\boldsymbol{M}(\boldsymbol{k})\,\boldsymbol{S}(\boldsymbol{k}) + \boldsymbol{S}(-\boldsymbol{k})\,\boldsymbol{M}^{T}(-\boldsymbol{k}) = -\boldsymbol{C}(\boldsymbol{k})\,. \tag{47}$$

From these equations, it is possible to theoretically derive the static and dynamic correlation functions. However, the expressions are lengthy ratios of sixth-order polynomials

J. Stat. Mech. (2025) 123206

and thus not given explicitly. Note,however, that by adiabatically integrating the temperature field, simpler expressions can be obtained (see appendix F).

It is insightful to provide some asymptotic analysis in the case where $\gamma \neq 0$:

$$\frac{\boldsymbol{S}_{\rho\rho}(k)}{\rho_0} \sim \begin{cases} \dfrac{G_T T_0 \eta_0^{\parallel}}{\gamma\rho_0 \left(G_T p_\rho - G_\rho p_T\right)} k^2 & \text{as } k \to 0 \\ \dfrac{T_0}{p_\rho} & \text{as } k \to \infty \end{cases} \tag{48}$$

$$\boldsymbol{S}_{u_\parallel u_\parallel}(k)\,\rho_0 \sim \begin{cases} \dfrac{T_0 \eta_0^{\parallel}}{\gamma\rho_0} k^2 & \text{as } k \to 0 \\ T_0 & \text{as } k \to \infty \end{cases} \tag{49}$$

$$\boldsymbol{S}_{u_\perp u_\perp}(k)\,\rho_0 \sim \begin{cases} \dfrac{T_0 \eta_0^{\perp}}{\gamma\rho_0} k^2 & \text{as } k \to 0 \\ T_0 & \text{as } k \to \infty \end{cases} \tag{50}$$

$$\boldsymbol{S}_{TT}(k)\,\rho_0 \sim \begin{cases} g\left(T_0, \gamma, \dots\right) k^2 & \text{as } k \to 0 \\ T_0^2 & \text{as } k \to \infty \end{cases} \tag{51}$$

with g being a complicated function. We recover the equilibrium results in the limit $k \to \infty$; however, at low k, we depart from the equilibrium result, notably by having expressions with transport coefficients appearing. Moreover, as seen in equation (48), we find strong hyperuniformity [95, 181–186]: $\boldsymbol{S}_{\rho\rho}(k) \sim k^2$. This is directly linked to the fact that the noise locally conserves the momentum while the damping does not, and is reminiscent of long-range correlations induced by bulk conservation law and boundary dissipation in self-organized criticality [166, 187–196]. See [197] for a recent review. This hyperuniformity in a crystal allows the breakdown of the Mermin–Wagner theorem [198–201].

For the dynamic correlation functions, asymptotic behavior is less interesting since most of the relevant physics occurs at intermediate frequencies, where sound propagates. However, we will make use of the asymptotic relation:

$$\boldsymbol{S}_{\rho\rho}(k, w) = 2T_0 \eta_0^{\parallel} (k/w)^4 \text{as } w \to \infty, \tag{52}$$

which can be derived from equation (46). Another interesting limit is given by $w \to 0$:

$$\boldsymbol{S}_{\rho\rho}(k, 0) \simeq \frac{2T_0}{\rho_0^2} \frac{\kappa_0 T_0 p_T^2 n_0^2 k^2 + G_T \eta_0^{\parallel} n_0 \rho_0^2 \left(G_T n_0 - 2\kappa_0 k^2\right)}{\left(G_T n_0 p_\rho - G_\rho n_0 p_T - p_\rho \kappa_0 k^2\right)^2}. \tag{53}$$

At equilibrium, when $G = 0$, we recover $\boldsymbol{S}_{\rho\rho}(k, 0) \sim k^{-2}$ as $k \to 0$ [202]. However, in our non-equilibrium setting, this scaling is not verified and at small k, $\boldsymbol{S}_{\rho\rho}(k, 0)$ reaches a plateau. It was postulated in [95] that this plateau could be used to facilitate the experimental detection of random-organizing hyperuniform fluid. As illustrated by the scaling in equation (53), this phenomenon is not exclusive to hyperuniform fluids, but is characteristic of systems with a rapidly relaxing temperature field due to its non-conservation. Indeed, it would be observed for a system without damping γ (and

J. Stat. Mech. (2025) 123206

thus non-hyperuniform) but with a nonconserved temperature field ($G_T \neq 0$) due to an energy change at collision; for example, with $\Delta \neq 0$, $\alpha < 1$ and $\gamma = 0$.

Note that at equilibrium, due to the fluctuation dissipation theorem, the static correlation functions at small k are easily obtained because $\boldsymbol{F}(k, t = 0)$ is known. Therefore, the dynamic correlation functions can be found without having to explicitly define a noise [164].

5.4. Numerical results

We performed simulations of our system and determined the different correlation functions by computing $\boldsymbol{F}(\boldsymbol{k}, t)$. Given the isotropic nature of our system, we averaged over a range of wavevectors $\boldsymbol{k}$ with similar magnitudes $k = |\boldsymbol{k}|$ and fitted the resulting function to a sum of complex exponentials, from which we subsequently took the Fourier transform. This procedure is necessary to obtain a smooth non-oscillating Fourier transform, as $\boldsymbol{F}$, being an autocorrelation function, is inherently noisy. However, we consistently verified that the fitting (used as a smoothing method) did not introduce any artifacts.

In figure 10(b), we provide the dynamic structure factor as a function of w for a given k and temperature. We only present the correlation functions at $w > 0$ since they are even. The theoretical prediction from equation (46) is included as a dashed line. Additionally, in figure 10(c), we present, in the main figure, the static structure factor, and in the inset, the longitudinal velocity-velocity static correlation for the same systems as those studied in panel (b). To provide an overview of the peculiarities and similarities between the system of interest and typical fluids, we present these correlation functions for four different systems:

- 'Equilibrium' is a simple equilibrium hard disk system. Its dynamic structure factor (panel (b)) exhibits three peaks [203] (only two are visible since we only show positive values of w): the Rayleigh peak at $k = 0$, related to heat diffusion and to the heat mode, and the Brillouin peaks at $w = \pm w_s(k_0)$, related to propagating sound waves. The structure factor (panel (c)) and static longitudinal velocity correlation (inset of panel (c)) are almost flat. The theory works flawlessly in this case [164]. Note that, at larger k, we expect a non-flat structure factor, for example, with a shape given by the Ornstein–Zernike theory of liquids [164].
- Here, 'Δ alone' is a non-equilibrium system with $\alpha < 1$, $\Delta > 0$ but $\gamma = 0$, which was thoroughly studied in [94]. Due to the nonconservation of energy in this system at collision (the particles still undergo a ballistic free flight with constant velocity), the Rayleigh peak in the dynamic structure factor begins to disappear. At lower k or lower α, it would not be visible at all, and only the Brillouin peak would be observable since sound can still propagate due to the conservation of momentum and density. This shows that even if the temperature field is technically a fast field because it is not conserved, it is still necessary to take it into account in the hydrodynamic description to qualitatively describe the observation since its relaxation time becomes comparable to those of the other fields at intermediate k. This regime was called quasi-elastic in [94]. Moreover, while at this wavevector $\boldsymbol{S}_{\rho\rho}(k, w)$ has an equilibrium-like shape with a Rayleigh peak, the corresponding static correlation functions are highly

J. Stat. Mech. (2025) 123206

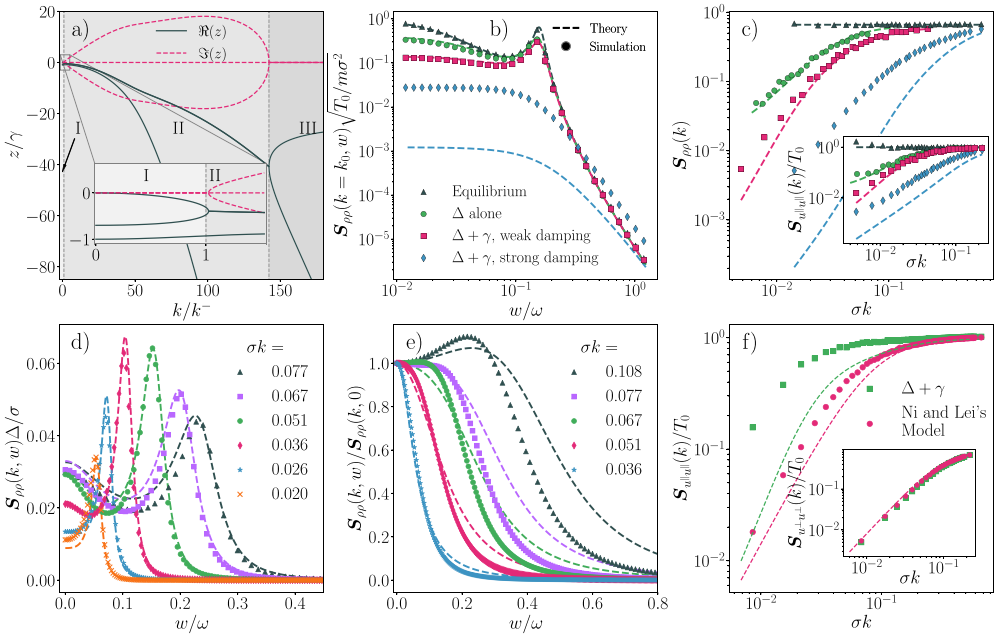

Figure 10. (a) Typical eigenvalues z of the hydrodynamic matrix $\boldsymbol{M}(k)$ (equation (40)) as a function of k. The trivial transverse mode is omitted. The dashed lines are the imaginary part of z while the solid lines are their real part. We see three typical regions, I and III where sound cannot propagate (z are purely real) and II, at intermediate k, for which sound is present. The inset is a zoom-in on region I, normalized by the theoretical wavenumber at which we expect a bifurcation k^-. $\phi = 0.3$, $(\Delta/\gamma\sigma) = 1.5$. (b) The theoretical (dashed lines) and measured (dots) dynamic structure factor $\boldsymbol{S}(k,w)$ as a function of w for different systems. We provide only $w > 0$ since the function is even. For each system the parameters are chosen to keep the kinetic temperature roughly constant; we also take $\phi = 0.1$ and $\sigma k_0 = 0.046$. 'Equilibrium' is a system of hard disks. For each non-equilibrium system, the temperature is fixed to the same value by varying Δ and γ while keeping $\alpha = 0.95$. Here, 'Δ alone' is a system without γ; '$\Delta+\gamma$, weak damping' is $\Delta/(\sigma\gamma) = 3.4$; '$\Delta+\gamma$, strong damping' is $\Delta/(\sigma\gamma) = 2.86$ and the system is starting to enter into the critical region. (c) The structure factor for the four systems considered in (b). The inset is the longitudinal velocity-velocity static correlation function. (d) Evolution of the dynamic structure factor as k is varied for the '$\Delta+\gamma$, weak damping' system. (e) Evolution of the dynamic structure factor as k is varied for the '$\Delta+\gamma$, strong damping' system. (f) Comparison of the theory and the simulations between the model introduced in [95] and our model for the longitudinal velocity-velocity static correlation function, and the transverse one in the inset. In both systems, $\alpha = 1$ and $\phi = 0.05$. For our system,$\Delta/(\sigma\gamma) = 7.67$. For Lei and Ni's model, $\Delta E/m(\sigma\gamma)^2 = 1388$. These choices of parameters lead to approximately the same temperature for both systems. In all cases, N varies between 5×10^4 and 1.5×10^6.

J. Stat. Mech. (2025) 123206

out of equilibrium and display a sharp decrease at low k. It should be emphasized that this system is not hyperuniform. Specifically, we can prove that without γ, contrary to the asymptotics found for $\gamma \neq 0$ in equations (48), the structure factor reaches a finite value. A derivation of this fact is provided in appendix F.

- Here, '$\Delta + \gamma$, weak damping' is the system studied in the main part of this article. Due to the additional source of energy dissipation ($\gamma \neq 0$) compared to the previous system, the Rayleigh peak has almost completely disappeared. We note that sound peaks are still visible. This indicates that with the chosen k_0, we fall into region II of figure 10(a). The structure factor and longitudinal velocity correlations are again well predicted, except at small k. We note that the k_0 used in panel (b) corresponds to a wavevector where the structure factor in panel (c) is well predicted. As a final remark, we find, as expected, the hyperuniformity $\boldsymbol{S}_{\rho\rho}(k) \sim k^2$ resulting from the interplay between the momentum conserving noise and the global damping predicted from the theory.
- Here, '$\Delta + \gamma$, strong damping' is the same system as the previous system, except with significantly increased damping, placing us at the boundaries of the critical region. Here, the sound modes have completely disappeared due to strong non-conservation of momentum. Additionally, the theoretical predictions fail. This failure might be in part attributed to the small population of inactive particles not taken into account in the hydrodynamic slow modes and the slight non-Gaussianity of the velocity distribution. However, a more rigorous analysis indicates that the theoretical framework consistently exhibits deviations with the simulations when $\gamma \neq 0$, although less pronounced, below a specific k where γ emerges as the predominant dissipative mechanism. This is why the density structure factor starts to deviate for the '$\Delta + \gamma$, weak damping' model below a given k. This is the inverse length at which the effect of γ becomes strong compared to the effects of α and Δ. In these cases, the velocity distribution is almost perfectly Gaussian and the discrepancies between simulation and theory cannot be attributed to our Gaussian assumptions. We again note the strong hyperuniformity of the structure factor and of the longitudinal static correlation function. However, the critical hyperuniform scaling $\boldsymbol{S}_{\rho\rho} \sim k^{0.5}$ is not observed at all, meaning that we are still far away from the transition.

In the following, we aim to understand the limitations of our model and its region of validity. In figure 10(d), we present the evolution of the dynamic structure factor for the '$\Delta + \gamma$, weak damping' system as k is varied. At large k, the theory works well, except at $w = 0$; this is likely due to the hydrodynamic approximation requiring a small k since the same departure from the theory is observed for the 'equilibrium' system (not shown). Additionally, although not easily visible in the structure factor in figure 10(c), the theory slightly deviates for these wavevectors, resulting in disagreement for the dynamic structure factor. At intermediate k, the theory agrees perfectly with the simulations. Decreasing the wavevector again makes us fall into the region dominated by γ, where neither the structure factor nor the dynamic structure factor are well predicted. We also note that for the smallest k, we see the Brillouin's peak decreasing as we approach region I.

J. Stat. Mech. (2025) 123206

In figure 10(e), we give the evolution of the dynamic structure factor for the '$\Delta+\gamma$, strong damping' system as k is varied. However, in this case, we know that the theory is completely wrong, partially because of the non-Gaussianity of the velocity distribution function but probably also due to additional effects not taken into account in the theory. We therefore normalize the dynamic structure factor by $\boldsymbol{S}_{\rho\rho}(k,0)$; this helps us eliminate, in part, the issue induced by a wrong prediction of the structure factor. At equilibrium, we could completely factorize the dynamic structure factor into a part that is independent of the noise used due to the fluctuation dissipation theorem. Indeed, the quantity $\boldsymbol{S}_{\rho\rho}(k,w)/\boldsymbol{S}_{\rho\rho}(k)$ would be purely computable from $\boldsymbol{M}$ without the need to include a noise term. In this non-equilibrium system, $\boldsymbol{S}_{\rho\rho}(k,0)$ is also related to $\boldsymbol{S}_{\rho T}(k)$ in a non-trivial way and the same argument cannot be made. This will, however, provide useful information. We see that while the theory does not quantitatively predict the results from the simulations, it ably captures the change in region from II to I as k is decreased. This leads us to conclude that the equilibrium noise we chose may be wrong, although the expressions for the transport coefficients are roughly correct.

Based on [95], these results are quite surprising. In this study, a similar model was used where a constant energy ΔE is injected at collision instead of relying on a constant velocity injection Δ, as in our case. Our systems are equivalent at the level of the density and momentum field but differ at the level of the temperature field due to different G:

$$\begin{aligned} G^{\text{Lei and Ni}} &= \omega(\phi,T)\,\Delta E - 2\gamma T \\ G^{\Delta+\gamma} &= \omega(\phi,T)\,\langle m\Delta^2 + \alpha m\,(\mathbf{v}_{ij}\cdot\hat{\boldsymbol{\sigma}}_{ij})\,\Delta - m\frac{1-\alpha^2}{4}\,(\mathbf{v}_{ij}\cdot\hat{\boldsymbol{\sigma}}_{ij})^2\rangle_{\text{coll}} - 2\gamma T \end{aligned}. \tag{54}$$

As clearly visible in these equations, our energy injection depends on the kinematic of the impact (and thus, on the temperature after the average on the collisions) while this is not the case in the system introduced in [95].

Surprisingly, with only the density and velocity fields, Lei and Ni obtained very good agreement between their simulations and the theory in the strong damping case (where the temperature is a fast field). This raises the question: why does our theory—which incorporates the temperature field in addition to the momentum and density fields—not work in our system, despite performing very well in the system studied by Lei and Ni? In figure 10(f), we present a comparison of simulations between their model and ours at the same density, damping and coefficient of restitution (in both cases $\alpha=1$ and all the dissipation is dealt by γ). We fixed Δ in our system and ΔE in theirs such that the temperature in both systems is the same. We also verified that the velocity distributions in both systems are similar and almost perfectly Gaussian (not shown). In the main panel, we provide measurement of the longitudinal static correlation function for both models alongside the predictions from the theory. The theory works fairly well for the model by Lei and Ni up to a factor of around 1.5. However, it completely fails for our system. From equation (49), we know that according to the theory, the low k longitudinal static velocity correlation function is proportional to the longitudinal viscosity $\eta_0^{\parallel}$; this suggests that the equilibrium viscosity coefficient used in the theory is not the right one, especially in our model. This disagreement between the two models

J. Stat. Mech. (2025) 123206

also holds for the structure factor (not shown). Interestingly, the models agree for the transverse velocity correlation function, as seen from the inset of figure 10(f). Since, for this observable, the theory works well, we are led to assert that the shear viscosity of both systems is very close to the equilibrium one used in the theory. Indeed, the low k transverse static velocity correlation is proportional to $\eta_0^{\perp} = \eta_0$. From this figure alone, we would thus be encouraged to think that the discrepancies between the two systems and between the theory and our system are solely due to the value of the longitudinal viscosity $\eta_0^{\parallel} = \eta_0 + \zeta_0$ used in the theory, and thus, the value of the bulk viscosity ζ_0 since the measured η_0 from the transversal correlation function seems consistent with the equilibrium one used in the theory. This would imply a bulk viscosity of an order of magnitude larger than the shear viscosity.

Nonetheless, from equation (52), we also predict that the large w tail of the dynamic structure factor is proportional to $\eta_0^{\parallel}$. But we see that this tail is very well predicted by the theory for the '$\Delta + \gamma$, weak damping' model in figure 10(b), implying that from this observable we are using a correct value for the longitudinal viscosity. Moreover, we remark that according to the theory (equations (F14) and (53)) both $\boldsymbol{S}_{\rho\rho}(k_0, w \to 0)$ and $\boldsymbol{S}_{\rho\rho}(k_0, w \to \infty)$ should be proportional to $\eta_0^{\parallel}$, which implies that, if the viscosity was the issue, we should observe discrepancies of similar orders of magnitude at $w = 0$ and $w \to \infty$, which is not the case.

In short, following the theory with the equilibrium noises, two different measurements of the longitudinal viscosity lead to two different values. This hints at a potential flaw in the choice of noises used.

An exact understanding of the root of the issue would require more work and is a very interesting question. It tells us that in systems where the energy is injected at collision, a slight difference in the method of energy injection can completely change the structural properties of the system. It also indicates that the assumption of an equilibrium like noise is generally unjustified, or that the transport coefficients can be strongly affected by the nature of the collisions. We also note that only data at small densities were presented, but due to the Enskog's correction, the theory works very well at higher densities (densities up to $\phi = 0.5$ were tested, see figure 14).

In this section, we only analyzed the 2D system. A similar analysis could be performed for the realistic quasi-2D model. Analysis (not shown) indicates that the dynamic structure factor obtained in the realistic quasi-2D model is consistent with the picture given for the effective 2D model; however, there are differences concerning the structure factor. In the realistic quasi-2D model, the structure factor never shows a strong $\boldsymbol{S}_{\rho\rho}(k) \sim k^2$ hyperuniformity. This is explained by the lack of conservation of the center of mass of the noise. In an idealized quasi-2D system, the global damping is due to tangential friction happening at each grain–plate collision. Thus, the damping is applied stochastically and discretely. Compared to the idealized global damping of the effective 2D model, this does not conserve the position of the center of mass and, as was demonstrated in [198], forbids true hyperuniformity. In an experimental system, the roughness of the plate would also affect the dynamics and would be the most important effect. A particle would act closely to a Brownian particle and a global noise would be effectively applied [204, 205], forbidding hyperuniformity [198].

J. Stat. Mech. (2025) 123206

Finally, the dynamic structure factor of the system close to the transition would merit further investigations. However, this is a topic for a separate study. Regardless, the results are expected to diverge significantly from the predictions of a simple linear theory. Indeed, in the vicinity of the transition, even a Gaussian theory going beyond the mean field is unable to predict the critical induced hyperuniformity [116]. Consequently, a renormalization group approach is necessary for a comprehensive understanding of the underlying physics [116].

6. Conclusion

In this work, we conducted an in-depth investigation of the system introduced in [55]. We demonstrated that an absorbing phase transition can occur in a granular system, with the nature of the transition determined by the presence or absence of synchronization. Building upon our previous findings, we analyzed, in greater detail, the structural properties of the system, both near the transition and within the active phase. We found that the critical point of the continuous transition exhibits a highly heterogeneous steady state, characterized by avalanche dynamics and non-trivial correlations, with critical exponents consistent with those of the conserved directed percolation universality class. In contrast, the discontinuous transition displays a more homogeneous state up to the onset of nucleation, which subsequently drives the system into a cooling regime reminiscent of free granular cooling and its associated instabilities. Furthermore, the active state of the corresponding two-dimensional effective model was shown to possess long-range correlations and to display hyperuniformity. Building on the theoretical framework established in [55], we derived, from the microscopic degrees of freedom, the field theory of the conserved directed percolation for our particle system, enabling a quantitative prediction of the homogeneous asynchronized state close to and far from the transition. By incorporating synchronization at the mean-field level, we also quantitatively captured the discontinuous transition. Finally, by including fluctuations around the homogeneous state, our extended theory successfully accounts for all observed correlation functions of the non-equilibrium liquid, as well as its emergent hyperuniformity.

Future work will focus on a more detailed experimental analysis to further validate the universality of our findings. Numerical investigations are still needed to better understand the tricritical point and the nucleation pathway in this system.

Acknowledgments

This work has been done with the support of Investissements d'Avenir of LabEx PALM (Grant No. ANR-10-LABX-0039-PALM). We thank Andrea Puglisi, Umberto Marini Bettolo Marconi and Lorenzo Caprini for fruitful scientific discussions concerning the fluctuating hydrodynamics of our model. We also thank Ran Ni for sharing with us their knowledge on the hyperuniformity in the metastable fluid and its relation to nucleation time. Finally, we are grateful to Yuta Kuroda for fruitful scientific discussions on hyperuniformity and fluctuating hydrodynamics.

J. Stat. Mech. (2025) 123206

Appendix A. Argument and potential derivation of the overpopulated tail of the velocity distribution

We follow [118, 119, 156] to derivate an overpopulated tail in granular medium. We adapt their argument to potentially explain the overpopulated tail observed close to the continuous transition in figure 7. We note, however, that the physical mechanism leading to this overpopulated tail is different in the simple granular cooling and in our case.

We start from the Boltzmann equation in our system, equation (31), and focus on large velocities $v_i \gg \Delta$. At high velocities, the only terms that will contribute to the probability change are the viscous damping drift $\gamma\partial/\partial\boldsymbol{v}\cdot(\boldsymbol{v}f)$ and the collisional gain term (the first term in equation (32)). The collisional loss term is negligible, as particles primarily cool down due to drag rather than collisions. Hence, in the steady state, assuming homogeneity, we can write down the following approximated Boltzmann equation:

$$-\gamma\frac{\partial}{\partial\boldsymbol{v}_i}\cdot(\boldsymbol{v}_i f)\simeq\chi\sigma\int\mathrm{d}\boldsymbol{v}_j\int\mathrm{d}\hat{\boldsymbol{\sigma}}_{ij}\Theta\left(\boldsymbol{v}_{ij}\cdot\hat{\boldsymbol{\sigma}}_{ij}-2\Delta\right)\left(\boldsymbol{v}_{ij}\cdot\hat{\boldsymbol{\sigma}}_{ij}-2\Delta\right)\frac{f\left(\boldsymbol{v}_j''\right)f\left(\boldsymbol{v}_i''\right)}{\alpha^2}. \quad \text{(A1)}$$

We proceed by noting that since the considered particle i has a large velocity v_i, it will on average collide with particles of smaller velocity. Consequently, $\boldsymbol{v}_{ij}\simeq\boldsymbol{v}_i$ and $\boldsymbol{v}_{ij}\cdot\hat{\boldsymbol{\sigma}}_{ij}-2\Delta\simeq\boldsymbol{v}_i\cdot\hat{\boldsymbol{\sigma}}_{ij}$. For ease of theoretical computation and to deal with the post collisional velocities, we focus on 1D systems where we do not expect any differences for the velocity distribution in simulations. We further simplify the problem by setting $\alpha=1$ since the same overpopulated tail is also obtained in an elastic system [95]. These assumptions for positive v_i lead to:

$$-\gamma\frac{\partial}{\partial v_i}\left(v_i f\right)\simeq 2\chi\sigma\left(v_i f\left(v_i\right)\right), \quad \text{(A2)}$$

which admits as a solution:

$$f\left(v\right)=Z\mathrm{e}^{-\beta v}-\log\left(v\right) \quad \text{(A3)}$$

with $\beta=2\chi\sigma/\gamma$ and Z is an integration constant. Equation (A3) demonstrates the potential development of an exponential overpopulated tail. However, a rigorous numerical and theoretical analysis are necessary to validate our approximations. Notably, the assumption of homogeneity is uncontrolled, as we saw that the population of active particle has a drastic effect on the global temperature of the system. Moreover, 1D systems are known to exhibit peculiar thermalization [206–210]. For example, a system of 1D hard elastic particles would never reach equilibrium because the collision rule would simply exchange the velocities of the colliding particles. A Gaussian velocity distribution would never be reached and the initial distribution would be conserved. With our non-equilibrium collision rule, a 1D fluid can equilibrate. However, there might still be

J. Stat. Mech. (2025) 123206

some differences compared to the 2D case, particularly regarding the efficiency of the energy spreading.

Verifying our proposition is not the main concern of the paper; we thus left this investigation for further studies.

Appendix B. Critical hyperuniform scaling for $S_{u^{\parallel}u^{\parallel}}(k)$ and $S_{u^{\perp}u^{\perp}}(k)$

In figure 11, we present the well-established hyperuniform scaling of the structure factor $S_{\rho\rho}(k)$ at the critical point. More unexpectedly, we also observe hyperuniform scaling for the longitudinal and transverse velocity correlation functions. Specifically, the longitudinal velocity correlation function decays as a power law $\sim k^{0.85}$ over an appreciable range of k. One might have anticipated that near the critical packing fraction ϕ_c, the only relevant fields would be the number of active particles and the density, leading to trivial velocity correlations. However, this is not the case. Remarkably, the transverse velocity field also exhibits hyperuniform scaling, decaying approximately as $\sim k^{1.95}$, which is consistent with the expected $\sim k^2$ scaling induced by the interplay between a global damping and a noise conserving the center of mass of the system, as described in section 5. In the linear regime—expected to break down near the transition—this scaling is indeed anticipated for the transverse velocity field.

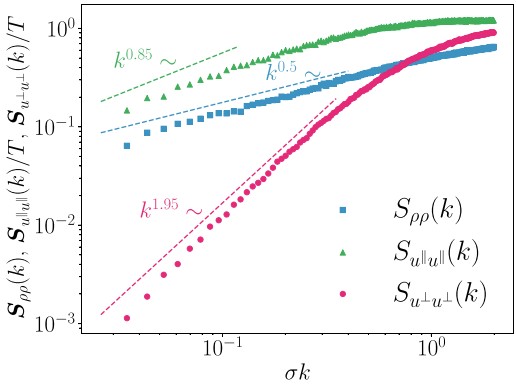

Figure 11. $S_{\rho\rho}(k)$, $S_{u^{\parallel}u^{\parallel}}(k)$ and $S_{u^{\perp}u^{\perp}}(k)$ as a function of k close to the critical point: $N = 10^5$, $\alpha = 0.95$, $\Delta/(\sigma\gamma) = 1.5$ and $\phi = 0.1512$.

Appendix C. Hyperuniform and clustered metastable fluids

The model presented in [104, 105] is similar to ours. While it does not contain synchronization, the collision dynamics is effectively similar to ours. In their model, if two particles collide with an energy smaller than a certain threshold, then the particles undergo elastic collision; otherwise they gain a finite amount of energy. A viscous drag is also applied during the free flight. In our model, particles that do not have a lot of energy are, on average, those which traveled for a long time and are slowed down

J. Stat. Mech. (2025) 123206

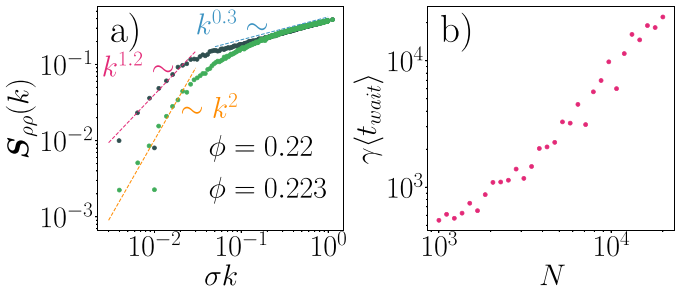

Figure 12. (a) The structure factor as a function of k for our system with synchronization but with $\alpha = 1$ at $\phi = 0.22$, $N = 10^6$ (very close to the transition packing fraction) and $\phi = 0.223$, $N = 4 \times 10^5$ (almost stable). (b) The average waiting time for the metastable state ($\phi = 0.22$) to reach the absorbing state as a function of the number of particles in the system. The average is performed over 20 independent runs. $1/(\gamma\tau_s) = 4.33$ and $\Delta/(\gamma\sigma) = 1.33$.

due to drag. Hence, they are likely to be synchronized and will therefore undergo collisions with $\Delta = 0$. This might mimic the effect of the energy-activated active collision of the models studied by Lei *et al.* Thus, the rough phenomenology of both models is similar, even though [104, 105] do not consider dissipative collisions, and drag is *de facto* their only source of dissipation. Interestingly, they find that the pathway of the metastable fluid to the absorbing state is seemingly not driven by a nucleation process but by large wavelength fluctuations, which are suppressed due to the non-equilibrium nature of the system. Indeed, they find that the metastable fluid has suppressed density fluctuations. On this basis, they argue that the non-equilibrium equivalent of the equilibrium metastable state becomes kinetically stable in the thermodynamic limit, due to the suppression of large wavelength fluctuations. The shrinking of the metastable region with system size is also observed using the minimal field theory of the conserved directed percolation universality class, modified to obtain a first-order transition [53, 106]. This is in disagreement with our results, as well as what was found in [33]. We believe the discrepancy is caused by the presence of dissipative collisions in our system that induces the formation of clusters, which enhance long-wavelength fluctuations and allow the regular nucleation pathway to the transition. Indeed, in contrast to [105], where dissipation arises solely from viscous drag, our model with $\alpha < 1$ includes dissipative collisions, which are responsible for driving the system to the absorbing state. The purely dissipative collisions between synchronized particles cause clustering, therefore inducing a peak at a wavevector k^* in the structure factor of the metastable fluid. These clusters appear to aid the system in reaching an absorbing state via a mechanism equivalent to equilibrium nucleation. Indeed, the system size L^*, at which a sharp drop in waiting time is found in figure 6, corresponds roughly to $2\pi/k^*$. However, it remains highly unclear why such phenomena facilitate the transition.

J. Stat. Mech. (2025) 123206

We now turn our analysis to a metastable fluid with a discontinuous transition but with $\alpha = 1$. In figure 12(a), we present the structure factor in the metastable regime (close to the discontinuous transition) in our model, but with $\alpha = 1$ where collisions are elastic, and therefore clustering does not occur. In contrast to the metastable fluid with $\alpha \neq 1$ (figure 7), we do not observe any peak in the structure factor. Instead, a hyperuniform scaling close to $k^{1.2}$ (but not incompatible with k^2 scaling at lower k) is visible for the metastable fluid ($\phi = 0.22$), in agreement with the results from [105]. We also note that a very long $k^{0.3}$ scaling is observed close to the metastable fluid. Additionally, the average waiting time $\langle t_{\text{wait}} \rangle$ increases monotonically with system size (or N), as shown in figure 12(b). This is in contrast with the non-monotonic behavior observed in figure 6. Thus, when dissipative collisions are absent, our system behaves similarly to that studied in [105], allowing a hyperuniform scaling to emerge in the metastable fluid. This scaling seemingly prohibits nucleation in the limit $N \to \infty$.

Appendix D. Tricritical point and continuous transition with synchronization

As discussed in the main text, even with synchronization, we can observe a continuous transition because the synchronization time competes with a finite mean collision time in the active region. Thus, at a large but finite synchronization time τ_s, significantly longer than the minimum mean collision time in active regions, synchronization will not influence the transition, which remains continuous. A less straightforward example of a continuous transition at finite τ_s occurs when $\alpha \ll 1$, as illustrated in figure 13(a). Indeed, we observe that by decreasing α, the transition becomes continuous. The continuity of the transition is made explicit in figure 13(b), where a scale analysis is performed for $\alpha = 0.8$ and shows that the temperature of the last active steady state tends to approach 0 with increasing system size. While the theory cannot quantitatively predict this transition, it still gives a qualitative answer. As evidenced from equation (29), in the case of small α, a discontinuous transition is theoretically predicted to occur at a small T_a. However, the population of inactive particles will reach 0 before the theoretical discontinuous transition happens, leading to a continuous transition instead. Similar transitions have been investigated in sandpiles belonging to the conserved directed percolation universality class [53]. In those systems, the mean-field approximation has been shown to quantitatively fail considerably around the passage from the discontinuous to continuous transition; notably, it has been found that the continuous transition for a range of parameters, is fluctuation induced.

This behavior implies the existence of a non-equilibrium tricritical point in our system. Such a phenomenon has been documented and thoroughly investigated in a closely related system in [104]. It would be interesting to observe a tricritical point in the realistic system as well. It will require further exploration, for example, through the use of very inelastic beads, such as plastic ones. Note that a tricritical point has also been observed for the liquid–solid phase transition of a quasi-2D granular gas [74, 75, 211].

J. Stat. Mech. (2025) 123206

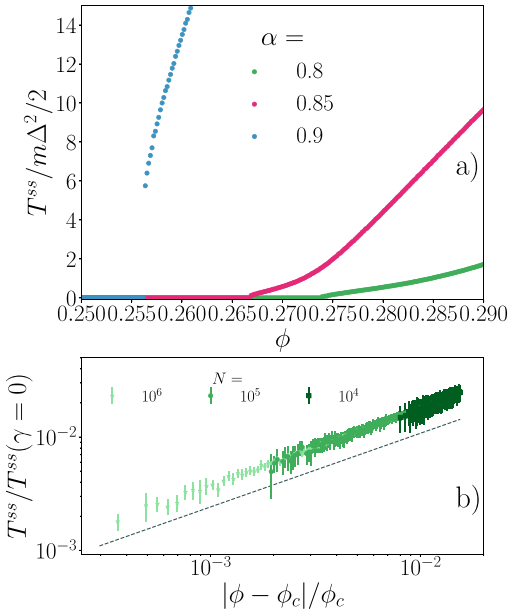

Figure 13. (a) Transition from the discontinuous to continuous transition with synchronization as α is decreased: $N = 10000$, $\Delta/(\gamma\sigma) = 2.5$ and $1/\gamma\tau_s = 25$. (b) A close-up of the transition for $\alpha = 0.8$ with a scaling analysis showing that the last active steady state ΔT_{ss} goes to 0 with system size, proving the continuity of the transition. The dashed line is the expected power law with the exponent from the conserved directed percolation universality class.

Appendix E. Expression for the transport coefficients and numerical values

As mentioned in the main text, we use the simple Enskog's equilibrium transport coefficients. They should give reasonable results in the active state. Moreover, while our simulations are mostly performed at $\phi = 0.1$, the theory works well at higher densities (see figure 14, where $\phi = 0.5$, for instance). Here, we provide a list of the expressions used. They are derived assuming molecular chaos and a Gaussian velocity distribution. We will also use the equilibrium contact value of the pair correlation function [129]:

$$\chi(\phi) = \frac{1 - 7\phi/16 - \phi^3/20}{(1-\phi)^2}. \tag{E1}$$

The pressure is given by [136]:

$$p = \rho T\left(1 + (1+\alpha)\,\phi\,\chi(\phi)\right) + 8\sqrt{\pi m}\phi\rho\chi(\phi)\,\Delta\sqrt{T}. \tag{E2}$$

J. Stat. Mech. (2025) 123206

The transport coefficients we used are the equilibrium ones from Enskog's theory [180]:

$$\begin{aligned}
\eta &= \frac{1}{2\sigma}\sqrt{\frac{mT}{\pi}}\left(\chi^{-1}+2\phi+(1+8/\pi)\,\chi\phi^2\right)\\
\zeta &= \frac{8\phi^2}{\sigma\pi}\chi\sqrt{\frac{mT}{\pi}}\\
\kappa &= \frac{2}{\sigma}\sqrt{\frac{T}{m\pi}}\left(\chi^{-1}+3\phi+(9/4+4/\pi)\,\chi\phi^2\right)\\
\mu &= 0\\
\nu &= 0
\end{aligned}\quad . \tag{E3}$$

For the transport coefficients, taking into account Δ and α, see [136]. The transport coefficients with $\Delta+\gamma$ are not known and should be derived from the Chapman–Enskog procedure.

Appendix F. Adiabatic slaving of the temperature field: $M^{(r)}$ and theoretical correlation functions

As already stated in the main text, we can find exact theoretical expressions for the eigenvalues of $\boldsymbol{M}$ or the dynamic and static correlation functions using equations (46) and (47). However, their expressions are not particularly useful since they are third-order polynomial roots or made of the ratio of polynomials of degree up to k^6. Therefore, it becomes necessary to perform approximations to make the computations more tractable and the results clearer. One way is to integrate the temperature field by assuming that it varies more quickly than any other field. This assumption is exact at $k=0$ since the others fields are conserved and hence have a relaxation timescale diverging with $1/k$. However, at larger k, this assumption will not be as good. Moreover, when $\gamma\neq 0$, the momentum field is also a fast field at small k. In what follows, we will only integrate the temperature field by following [94], in order to obtain a hydrodynamic description with only the velocity and density fields.

From equation (40), the evolution for the temperature field reads (we again drop the explicit evaluation of the derivative at the homogeneous state and the small transport coefficients μ_0 and ν_0):

$$\delta\dot{T}(t) = -\Gamma\delta T(t) + \mathcal{s}(t), \tag{F1}$$

with:

$$\Gamma(k) = -G_{\mathrm{T}} + \frac{\kappa_0}{n_0}k^2, \tag{F2}$$

$$\mathcal{s}(t) = G_\rho\delta\rho - \mathrm{i}k\frac{p_0}{n_0}\delta u_{\parallel} + \Xi_T(t) \tag{F3}$$

where Ξ_{T} is the noise on the temperature field defined in equation (45). A very crude approximation would be to set $\delta\dot{T}=0$. However, we can go further by formally solving

this equation, taking the disturbance due to $\delta\rho$ and $\delta u_{\parallel}$ as sources $\mathcal{S}(t)$ for δT, which is damped at a frequency Γ. Its solution is:

$$\delta T(t) = \int_{-\infty}^{t} \mathrm{d}t' \mathrm{e}^{\Gamma(t'-t)} \mathcal{S}(t'), \tag{F4}$$

with $\Gamma = -G_{\mathrm{T}} + \kappa_0 k^2/n_0 > 0$ is an inverse relaxation time for the temperature field and where we assumed $\delta T(-\infty) = 0$ without loss of generality since we are only concerned about the long time limit. We could then replace this solution for $\delta T(t)$ in the hydrodynamic equation given by $\dot{\boldsymbol{\Psi}} = \boldsymbol{M}\boldsymbol{\Psi}$. We would have eliminated the temperature field exactly, at the cost of having to deal with a non-Markovian system with an exponential kernel. At that point, it is possible to indeed follow this route, integrate the equations by parts and eventually perform an expansion on the resulting equation for the density and velocity. However, we follow [94] and immediately perform the adiabatic expansion on equation (F4) by performing successive integration by parts to expand the integral in powers of Γ^{-1}. Here, Γ is assumed to be large compared to the other relaxation scale due to its finiteness at $k = 0$, allowing us to truncate the expansion without significant loss of physical accuracy. The expansion is performed as follows:

$$\begin{aligned}
\delta T(t) &= \int_{-\infty}^{t} \mathrm{d}t' \mathrm{e}^{\Gamma(t'-t)} \mathcal{S}(t') \\
&= \left[\frac{\mathrm{e}^{\Gamma(t'-t)}\mathcal{S}(t')}{\Gamma}\right]_{-\infty}^{t} - \frac{1}{\Gamma}\int_{-\infty}^{t} \mathrm{d}t' \mathrm{e}^{\Gamma(t'-t)} \mathcal{S}'(t') \\
&= \sum_{n=0}^{N} \frac{(-1)^n}{\Gamma^{n+1}} \frac{\partial^n \mathcal{S}(t)}{\partial t^n} \\
&\quad + \sum_{m=N+1}^{\infty} \frac{(-1)^m}{\Gamma^m} \int_{-\infty}^{t} \mathrm{d}t' \mathrm{e}^{\Gamma(t'-t)} \frac{\partial^m \mathcal{S}(t)}{\partial t^m} \\
&= \frac{\mathcal{S}(t)}{\Gamma} - \frac{\dot{\mathcal{S}}(t)}{\Gamma^2} + \mathcal{O}\left(\Gamma^{-3}\right)
\end{aligned} \tag{F5}$$

Next, we will retain only the first two terms (up to the first time derivative) because the remaining terms contribute at orders higher than k^2 in the hydrodynamic equations. By doing this, we transformed the memory dependence into a derivative dependence, effectively rendering our equation Markovian. Naturally, an infinite series of derivatives is non-local; only the truncation at a finite order is Markovian. It is important to note that the first term of the expansion corresponds to $\delta\dot{T} = 0$, indicating that the second term, proportional to $\dot{S}$, introduces a genuinely non-instantaneous contribution.

By taking the derivative of $\mathcal{S}$ and inserting into it the hydrodynamic equations for $\delta\rho$ and $\delta u_{\parallel}$ we obtain:

$$\dot{\mathcal{S}}(t) = -i\left(\rho_0 G_\rho + \gamma p_0/n_0\right) k \delta u_{\parallel}(t) + \dot{\Xi}_T(t) + \mathcal{O}\left(k^2\right), \tag{F6}$$

J. Stat. Mech. (2025) 123206

where only terms up to the first order in k are kept because higher terms would contribute to the order $k^{n>2}$ in the hydrodynamic equations. The formal derivative of the white Gaussian noise has to be understood as a weak derivative in the sense of distributions. It has the following correlation:

$$\langle \dot{\Xi}_T(k,t)\,\dot{\Xi}_T(k',t')\rangle = -\frac{2\langle \Xi_T(k,t)\,\Xi_T(k',t')\rangle}{(t-t')^2}, \tag{F7}$$

or equivalently, in Fourier space:

$$\langle \dot{\Xi}_T(k,w)\,\dot{\Xi}_T(k',w')\rangle = w^2\langle \Xi_T(k,w)\,\Xi_T(k',w')\rangle. \tag{F8}$$

Note that these relations hold only when Ξ is a Gaussian white noise process.

Setting the noise to 0, and replacing all δT in the first two rows of $\boldsymbol{M}$ by the expression found in equation (F5), we find $\boldsymbol{M}^{(r)}$:

$$\boldsymbol{M}^{(r)}(k) = \begin{pmatrix} 0 & -\mathrm{i}\rho_0 k \\ -\dfrac{\mathrm{i}k}{\rho_0}\left(p_\rho - \dfrac{G_\rho p_\mathrm{T}}{G_\mathrm{T}}\right)\Big|_{\rho_0,T_0} & -\gamma - \left(\dfrac{\eta_0^{\parallel}}{\rho_0} - \dfrac{(G_\mathrm{T}-\gamma)(p_0+\nu_0)p_\mathrm{T}}{G_\mathrm{T}^2\rho_0 n_0} - \dfrac{G_\rho p_\mathrm{T}}{G_\mathrm{T}^2}\right)\Big|_{\rho_0,T_0} k^2 \end{pmatrix}. \tag{F9}$$

This reduced hydrodynamics model includes correction to the simple model introduced by Lei and Ni [95] to describe a hyperuniform fluid. The first stability criterion is again apparent here in the velocity–density coupling. Similar systems, with an effective Δ, were found to be unstable due to the positivity of this term [212, 213]. At equilibrium, spinodal instabilities related to phase transitions are also captured by the term $\boldsymbol{M}_{u^{\parallel}\rho}$ in a hydrodynamic theory, since the compressibility $1/(\rho p_\rho)$ becomes negative. However, such instability analysis on the hydrodynamic matrix cannot capture the binodals, metastability and coexistence densities, as these require thermodynamic information or additional constraints [214–218].

We now turn to correlation computation. Due to the peculiar correlation of the derivative of the white noise, it is not very practical to use the relations used in the main text to find $\boldsymbol{S}(\boldsymbol{k},w)$ and $\boldsymbol{S}(\boldsymbol{k})$ (equations (46) and (47)). Moreover, the adiabatic expansion in its impressive state starts to become heavy to carry since second derivatives of noises arise. To easily compute $\boldsymbol{S}(\boldsymbol{k},w)$ and $\boldsymbol{S}(\boldsymbol{k})$, we chose to ignore the time derivative contribution $\dot{S}(t)$ in the expansion of $\delta T(t)$, which involves simply setting $\delta\dot{T}=0$. This is inconsistent but leads to good results. For simplicity and for illustrative purposes, we will work in the case $\gamma=0$, which implies $G_\rho=0$. This allows us to nicely predict the observed shape of the structure factor for the system 'Δ alone' in figure 10. To continue, we take the derivative of $\delta\dot{u}_{\parallel}$:

$$\delta\ddot{u}_{\parallel}(t) = -p_\rho k^2\delta u_{\parallel}(t) - \frac{\eta_0^{\parallel}}{\rho_0}k^2\delta\dot{u}_{\parallel}(t) - \mathrm{i}k\frac{p_\mathrm{T}}{\rho_0}\frac{S(t)}{\Gamma} + \dot{\Xi}_{u_{\parallel}}(t). \tag{F10}$$

J. Stat. Mech. (2025) 123206

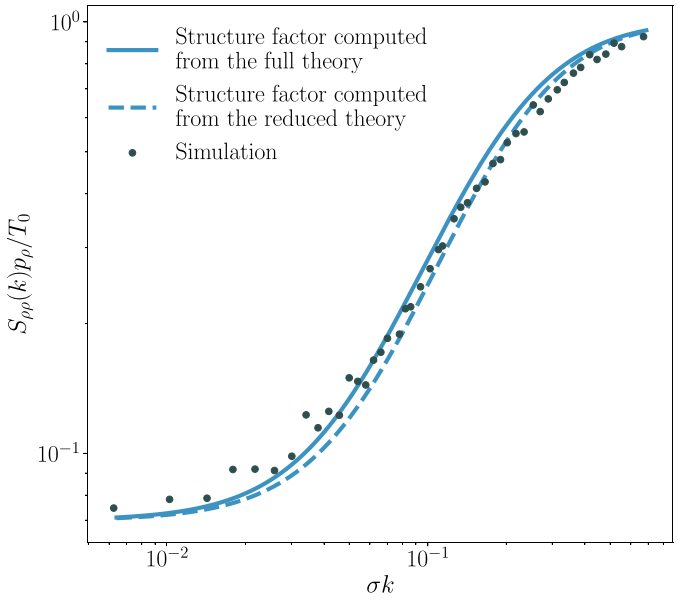

Figure 14. Comparison between the structure factor found in the simulations of the simple Δ model without damping, the full theory (obtained from the full hydrodynamic matrix) and the adiabatic slaving (equation (F14)): $\alpha = 0.9$, $\phi = 0.5$ and $N = 2.5 \times 10^6$.

Taking the Fourier transform of this equation and computing $\boldsymbol{S}_{u_\parallel u_\parallel}(k,w) = \langle u_\parallel(k,w) u_\parallel(-k,-w)\rangle$ leads to:

$$\boldsymbol{S}_{u_\parallel u_\parallel}(k,w) = \frac{\mu_{u_\parallel} + \mu_T}{\left(k^2 p_\rho - w^2\right)^2 + w^2 k^4 \left(\frac{p_0 p_{\mathrm{T}}}{\Gamma \rho_0 n_0} - \frac{\eta_0^\parallel}{\rho_0}\right)^2}, \tag{F11}$$

with $\mu_{u_\parallel}$ and μ_T related to the variance of the time derivative of the velocity and temperature field, respectively:

$$\begin{aligned} \mu_{u_\parallel} &= 2k^2 w^2 T \eta_0^\parallel / \rho^2, \\ \mu_T &= 2k^4 p_{\mathrm{T}}^2 T^2 w^2 \kappa / \left(\Gamma^2 \rho^4\right). \end{aligned} \tag{F12}$$

We can integrate between $-\infty$ and ∞ and divide equation (F11) by 2π to find the static correlation function. This gives the simple result:

$$\begin{aligned} \boldsymbol{S}_{u^\parallel u^\parallel}(k) \frac{\rho_0}{T_0} &= \boldsymbol{S}_{\rho\rho}(k) \frac{p_\rho}{\rho_0 T_0} \\ &= \frac{\kappa_0 k^2}{\kappa_0 k^2 + G_{\mathrm{T}} \rho_0} + \frac{G_{\mathrm{T}} \eta_0^\parallel \rho_0}{p_{\mathrm{T}}^2 T_0 + \eta_0^\parallel \left(\kappa_0 k^2 + G_{\mathrm{T}} \rho_0\right)}, \end{aligned} \tag{F13}$$

where the density structure factor was found using the density field hydrodynamic equation.

J. Stat. Mech. (2025) 123206

As with $\gamma \neq 0$, at large k we recover the equilibrium result. Nonetheless, when $G_{\mathrm{T}} \neq 0$, we see that the system has a transient hyperuniform scaling (first term) until it reaches a constant value given by:

$$\boldsymbol{S}_{\rho\rho}(0)/\rho_0 = \frac{T_0}{P_\rho}\left(1 - \frac{1}{1 + \dfrac{G_{\mathrm{T}}\eta_0^{\parallel}\rho}{p_{\mathrm{T}}^2 T_0}}\right). \tag{F14}$$

Interestingly, the equilibrium limit $G_{\mathrm{T}} \to 0$, which occurs, for example, when $\alpha \to 1$, is singular. Indeed, as we approach this singular equilibrium limit $\alpha \to 1$, the value of $S(0)$ decreases to 0, moving us further away from the true equilibrium result that is proportional to the temperature and the compressibility. However, as this limit is approached, increasingly smaller values of k are required for the transient hyperuniform scaling to manifest. This implies that infinitely close to the equilibrium limit, an infinitely large system is required to observe the non-equilibrium behavior of the structure factor. One might argue that our theoretical predictions become unreliable near equilibrium because the parameter T does not vary rapidly. However, it is important to note that a value of k will always exist for which the conserved fields ρ and $\boldsymbol{u}$ evolve more slowly than the non-conserved temperature field. Therefore, the asymptotic behavior remains reliable and, indeed, exact.

A comparison between simulations and theory is given in figure 14 for the structure factor. The reduced theory (that developed in this section, with the adiabatic slaving) works very well. Note here that $\alpha = 0.9$ and $\phi = 0.5$. It is satisfying that the theory still works at such high densities. At lower α, however, we would not expect such good agreement. Note also that we chose a reasonably small α and high densities because they both facilitate the observation of the transient hyperuniform scaling.

ORCID iDs

R Maire 0009-0007-7530-9626
A Plati 0000-0001-9317-6862
F Smallenburg 0000-0002-9401-6067
G Foffi 0000-0002-7444-1453

References

[1] Hinrichsen H 2000 *Adv. Phys.* **49** 815
[2] Lübeck S 2004 *Int. J. Mod. Phys. B* **18** 3977
[3] Mata A S 2021 *Chaos* **31** 012101
[4] Dickman R, Vespignani A and Zapperi S 1998 *Phys. Rev. E* **57** 5095
[5] Hinrichsen H, Jiménez-Dalmaroni A, Rozov Y and Domany E 1999 *Phys. Rev. Lett.* **83** 4999
[6] Hinrichsen H, Jiménez-Dalmaroni A, Rozov Y and Domany E 2000 *J. Stat. Phys.* **98** 1149
[7] Jo M, Lee J, Choi K and Kahng B 2021 *Phys. Rev. Res.* **3** 013238
[8] O'Dea N, Morningstar A, Gopalakrishnan S and Khemani V 2024 *Phys. Rev. B* **109** L020304
[9] Sierant P and Turkeshi X 2023 *Phys. Rev. Lett.* **130** 120402
[10] Chertkov E *et al* 2023 *Nat. Phys.* **19** 1799

J. Stat. Mech. (2025) 123206

[11] Marcuzzi M, Buchhold M, Diehl S and Lesanovsky I 2016 *Phys. Rev. Lett.* **116** 245701
[12] Ziff R M, Gulari E and Barshad Y 1986 *Phys. Rev. Lett.* **56** 2553
[13] Pine D J, Gollub J P, Brady J F and Leshansky A M 2005 *Nature* **438** 997
[14] Reichhardt C, Regev I, Dahmen K, Okuma S and Reichhardt C J O 2023 *Phys. Rev. Res.* **5** 021001
[15] Corte L, Chaikin P M, Gollub J P and Pine D J 2008 *Nat. Phys.* **4** 420
[16] Nagamanasa K H, Gokhale S, Sood A and Ganapathy R 2014 *Phys. Rev. E* **89** 062308
[17] Jeanneret R and Bartolo D 2014 *Nat. Commun.* **5** 3474
[18] Franceschini A, Filippidi E, Guazzelli E and Pine D J 2011 *Phys. Rev. Lett.* **107** 250603
[19] Keim N C and Arratia P E 2014 *Phys. Rev. Lett.* **112** 028302
[20] Tjhung E and Berthier L 2015 *Phys. Rev. Lett.* **114** 148301
[21] Tjhung E and Berthier L 2016 *J. Stat. Mech.* 033501
[22] Wilken S, Guerra R E, Pine D J and Chaikin P M 2020 *Phys. Rev. Lett.* **125** 148001
[23] Knowlton E D, Pine D J and Cipelletti L 2014 *Soft Matter* **10** 6931
[24] Weijs J H, Jeanneret R, Dreyfus R and Bartolo D 2015 *Phys. Rev. Lett.* **115** 108301
[25] Takeuchi K A, Kuroda M, Chaté H and Sano M 2007 *Phys. Rev. Lett.* **99** 234503
[26] Fiocco D, Foffi G and Sastry S 2013 *Phys. Rev. E* **88** 020301
[27] Regev I, Lookman T and Reichhardt C 2013 *Phys. Rev. E* **88** 062401
[28] Bhaumik H, Foffi G and Sastry S 2021 *Proc. Natl Acad. Sci.* **118** e2100227118
[29] Wilken S, Guo A Z, Levine D and Chaikin P M 2023 *Phys. Rev. Lett.* **131** 238202
[30] Wilken S, Guerra R E, Levine D and Chaikin P M 2021 *Phys. Rev. Lett.* **127** 038002
[31] Ness C and Cates M E 2020 *Phys. Rev. Lett.* **124** 088004
[32] Möbius R and Heussinger C 2014 *Soft Matter* **10** 4806
[33] Néel B, Rondini I, Turzillo A, Mujica N and Soto R 2014 *Phys. Rev. E* **89** 042206
[34] Vellela M and Qian H 2009 *J. R. Soc. Interface* **6** 925
[35] Schlögl F 1972 *Z. Phys.* **253** 147
[36] de Andrade M F and Figueiredo W 2023 *Phys. Lett. A* **475** 128863
[37] Garcia Lorenzana G, Altieri A and Biroli G 2024 *PRX Life* **2** 013014
[38] Pascual M and Guichard F 2005 *Trends Ecol. Evol.* **20** 88
[39] Clar S, Schenk K and Schwabl F 1997 *Phys. Rev. E* **55** 2174
[40] Chang S L, Harding N, Zachreson C, Cliff O M and Prokopenko M 2020 *Nat. Commun.* **11** 5710
[41] Jocteur T, Figueiredo S, Martens K, Bertin E and Mari R 2024 *Phys. Rev. Lett.* **132** 268203
[42] Bertin E, Andrix A and Le Godais G 2024 *J. Stat. Phys.* **191** 1
[43] Chantry M, Tuckerman L S and Barkley D 2017 *J. Fluid Mech.* **824** R1
[44] Gomé S, Rivière A, Tuckerman L S and Barkley D 2024 *Phys. Rev. Lett.* **132** 264002
[45] Hof B 2023 *Nat. Rev. Phys.* **5** 62
[46] Lemoult G, Shi L, Avila K, Jalikop S V, Avila M and Hof B 2016 *Nat. Phys.* **12** 254
[47] Jocteur T, Nardini C, Bertin E and Mari R 2025 arXiv:2506.14330
[48] Rossi M, Pastor-Satorras R and Vespignani A 2000 *Phys. Rev. Lett.* **85** 1803
[49] Le Doussal P and Wiese K J 2015 *Phys. Rev. Lett.* **114** 110601
[50] Martiniani S, Chaikin P M and Levine D 2019 *Phys. Rev. X* **9** 011031
[51] Kawasaki T and Berthier L 2016 *Phys. Rev. E* **94** 022615
[52] Leishangthem P, Parmar A D and Sastry S 2017 *Nat. Commun.* **8** 14653
[53] di Santo S, Burioni R, Vezzani A and Munoz M A 2016 *Phys. Rev. Lett.* **116** 240601
[54] Mari R, Bertin E and Nardini C 2022 *Phys. Rev. E* **105** L032602
[55] Maire R, Plati A, Stockinger M, Trizac E, Smallenburg F and Foffi G 2024 *Phys. Rev. Lett.* **132** 238202
[56] Fisher D S, Dahmen K, Ramanathan S and Ben-Zion Y 1997 *Phys. Rev. Lett.* **78** 4885
[57] Van Wijland F, Oerding K and Hilhorst H 1998 *Physica A* **251** 179
[58] Pires M A, Sampaio Filho C I, Herrmann H J and Andrade J S Jr 2023 *Chaos Solitons Fractals* **174** 113761
[59] Assis V R and Copelli M 2009 *Phys. Rev. E* **80** 061105
[60] de Oliveira M M, Alves S G and Ferreira S C 2016 *Phys. Rev. E* **93** 012110
[61] Jagla E A, Landes F m c P and Rosso A 2014 *Phys. Rev. Lett.* **112** 174301
[62] Cundall P A and Strack O D L 1979 *Géotechnique* **29** 47
[63] Pöschel T and Schwager T 2005 *Computational Granular Dynamics* (Springer)
[64] Thompson A P *et al* 2022 *Comput. Phys. Commun.* **271** 108171
[65] Kloss C and Goniva C 2010 *LAMMPS User Workshop*
[66] Plati A, Baldassarri A, Gnoli A, Gradenigo G and Puglisi A 2019 *Phys. Rev. Lett.* **123** 038002
[67] O'Sullivan C and Cui L 2009 *Powder Technol.* **193** 289

J. Stat. Mech. (2025) 123206

[68] Zhang H P and Makse H A 2005 *Phys. Rev. E* **72** 011301
[69] Plati A and Puglisi A 2022 *Phys. Rev. Lett.* **128** 208001
[70] Popov V L 2010 *Contact Mechanics and Friction* (Springer) (https://doi.org/10.1007/978-3-642-10803-7)
[71] Mindlin R D 2021 *J. Appl. Mech.* **16** 259
[72] LAMMPS developer 2024 *Pair Style Granular Command* (available at: https://docs.lammps.org/pair_granular.html)
[73] Reis P M, Ingale R A and Shattuck M D 2006 *Phys. Rev. Lett.* **96** 258001
[74] Castillo G, Mujica N and Soto R 2012 *Phys. Rev. Lett.* **109** 095701
[75] Castillo G, Mujica N and Soto R 2015 *Phys. Rev. E* **91** 012141
[76] Olafsen J S and Urbach J S 1998 *Phys. Rev. Lett.* **81** 4369
[77] Komatsu Y and Tanaka H 2015 *Phys. Rev. X* **5** 031025
[78] Pierański P 1983 *J. Phys.* **44** 573
[79] Pierański P, Kowalik Z and Franaszek M 1985 *J. Phys.* **46** 681
[80] Chastaing J-Y, Bertin E and Géminard J-C 2015 *Am. J. Phys.* **83** 518
[81] Mujica N and Soto R 2016 *Recent Advances in Fluid Dynamics With Environmental Applications* (Springer) p 445
[82] Schindler T 2023 Phase behavior and perturbation response of quasi-2D driven granulates employing molecular dynamics simulations *PhD Thesis* Friedrich-Alexander-Universität Erlangen-Nürnberg (FAU)
[83] Rivas N, Ponce S, Gallet B, Risso D, Soto R, Cordero P and Mujica N 2011 *Phys. Rev. Lett.* **106** 088001
[84] Everson R 1986 *Physica D* **19** 355
[85] Mehta A and Luck J M 1990 *Phys. Rev. Lett.* **65** 393
[86] Luck J M and Mehta A 1993 *Phys. Rev. E* **48** 3988
[87] Acebrón J A, Bonilla L L, Vicente C J P, Ritort F and Spigler R 2005 *Rev. Mod. Phys.* **77** 137
[88] Maynar P, García de Soria M and Brey J J 2019 *Phys. Rev. E* **99** 032903
[89] Maynar P, de Soria M G and Brey J J 2019 *J. Stat. Mech.* 093205
[90] Brey J J, de Soria M G and Maynar P 2019 *Phys. Rev. E* **100** 052901
[91] Brey J J, García de Soria M and Maynar P 2020 *Phys. Rev. E* **101** 012102
[92] Brey J J, Maynar P and de Soria M G 2020 *J. Stat. Mech.* 034002
[93] Mayo M, Petit J, de Soria M G and Maynar P 2023 *J. Stat. Mech.* 123208
[94] Brito R, Risso D and Soto R 2013 *Phys. Rev. E* **87** 022209
[95] Lei Q-L and Ni R 2019 *Proc. Natl Acad. Sci.* **116** 22983
[96] Smallenburg F 2022 *Eur. Phys. J. E* **45** 22
[97] Ódor G 2004 *Rev. Mod. Phys.* **76** 663
[98] van Wijland F 2002 *Phys. Rev. Lett.* **89** 190602
[99] Henkel M 2008 *Non-Equilibrium Phase Transitions* (Springer) (https://doi.org/10.1007/978-90-481-2869-3)
[100] Garzó V 2005 *Phys. Rev. E* **72** 021106
[101] Mitrano P P, Dahl S R, Cromer D J, Pacella M S and Hrenya C M 2011 *Phys. Fluids* **23** 093303
[102] McNamara S and Young W R 1994 *Phys. Rev. E* **50** R28
[103] Khain E and Aranson I S 2011 *Phys. Rev. E* **84** 031308
[104] Lei Q-L, Hu H and Ni R 2021 *Phys. Rev. E* **103** 052607
[105] Lei Y and Ni R 2023 *Proc. Natl Acad. Sci.* **120** e2312866120
[106] Buendía V, di Santo S, Villegas P, Burioni R and Muñoz M A 2020 *Phys. Rev. Res.* **2** 013318
[107] Bak P and Chen K 1991 *Sci. Am.* **264** 46
[108] Pruessner G 2013 *Int. J. Mod. Phys. B* **27** 1350009
[109] Manna S, Kiss L B and Kertész J 1990 *J. Stat. Phys.* **61** 923
[110] Wiese K J 2024 *Phys. Rev. Lett.* **133** 067103
[111] Torquato S 2018 *Phys. Rep.* **745** 1
[112] Torquato S 2016 *Phys. Rev. E* **94** 022122
[113] Salvalaglio M, Skinner D J, Dunkel J and Voigt A 2024 *Phys. Rev. Res.* **6** 023107
[114] Hexner D and Levine D 2015 *Phys. Rev. Lett.* **114** 110602
[115] Hexner D, Chaikin P M and Levine D 2017 *Proc. Natl Acad. Sci.* **114** 4294
[116] Ma X, Pausch J and Cates M E 2023 Theory of hyperuniformity at the absorbing state transition (arXiv:2310.17391)
[117] Yu P, Schröter M and Sperl M 2020 *Phys. Rev. Lett.* **124** 208007
[118] Esipov S E and Pöschel T 1997 *J. Stat. Phys.* **86** 1385
[119] Van Noije T and Ernst M 1998 *Granul. Matter* **1** 57
[120] Arnarson B O and Willits J T 1998 *Phys. Fluids* **10** 1324

J. Stat. Mech. (2025) 123206

[121] Jarzynski C and Swiatecki W 1993 *Nucl. Phys. A* **552** 1
[122] Singh R, Metzler R and Sandev T 2020 *J. Phys. A: Math. Theor.* **53** 505003
[123] Pal A 2015 *Phys. Rev. E* **91** 012113
[124] Goldhirsch I and Zanetti G 1993 *Phys. Rev. Lett.* **70** 1619
[125] Brey J J, Dufty J W, Kim C S and Santos A 1998 *Phys. Rev. E* **58** 4638
[126] Bray A J 1994 *Adv. Phys.* **43** 357
[127] Paul S and Das S K 2017 *Phys. Rev. E* **96** 012105
[128] Pagonabarraga I, Trizac E, Van Noije T and Ernst M 2001 *Phys. Rev. E* **65** 011303
[129] Mulero A, Cachadina I and Solana J 2009 *Mol. Phys.* **107** 1457
[130] van Noije T P and Ernst M H 2001 *Granular Gases* (Springer) pp 3–30
[131] Gardiner C 2009 *Stochastic Methods* vol 4 (Springer)
[132] Sarracino A, Villamaina D, Gradenigo G and Puglisi A 2010 *Europhys. Lett.* **92** 34001
[133] Van Noije T, Ernst M and Brito R 1998 *Physica A* **251** 266
[134] Visco P, van Wijland F and Trizac E 2008 *J. Phys. Chem. B* **112** 5412
[135] Manna S 1999 *Curr. Sci.* **77** 388
[136] Garzó V, Brito R and Soto R 2018 *Phys. Rev. E* **98** 052904
[137] Brey J J, de Soria M G, Maynar P and Buzón V 2013 *Phys. Rev. E* **88** 062205
[138] Goldenfeld N 2018 *Lectures on Phase Transitions and the Renormalization Group* (CRC Press) (https://doi.org/10.1201/9780429493492)
[139] Cardy J 1996 *Scaling and Renormalization in Statistical Physics* vol 5 (Cambridge University Press)
[140] Aron C and Kulkarni M 2020 *Phys. Rev. Res.* **2** 043390
[141] Aron C and Chamon C 2020 *SciPost Phys.* **8** 074
[142] Guislain L and Bertin E 2023 *Phys. Rev. Lett.* **130** 207102
[143] Ptaszynski K and Esposito M 2025 *Phys. Rev. E* **111** 044142
[144] Dornic I, Chaté H and Munoz M A 2005 *Phys. Rev. Lett.* **94** 100601
[145] Van Kampen N G 1992 *Stochastic Processes in Physics and Chemistry* vol 1 (Elsevier)
[146] Canet L, Chaté H and Delamotte B 2011 *J. Phys. A: Math. Theor.* **44** 495001
[147] Honkonen J 2011 arXiv:1102.1581
[148] Zakine R and Vanden-Eijnden E 2023 *Phys. Rev. X* **13** 041044
[149] Elgart V and Kamenev A 2004 *Phys. Rev. E* **70** 041106
[150] Meerson B and Sasorov P V 2011 *Phys. Rev. E* **83** 011129
[151] Assaf M and Meerson B 2017 *J. Phys. A: Math. Theor.* **50** 263001
[152] Pitaevskii L P and Lifshitz E 2012 *Physical Kinetics* vol 10 (Butterworth-Heinemann)
[153] Mazenko G 2006 *Nonequilibrium Statistical Mechanics* (Wiley) (https://doi.org/10.1002/9783527618958)
[154] Kardar M 2007 *Statistical Physics of Particles* (Cambridge University Press) (https://doi.org/10.1017/CBO9780511815898)
[155] Brey J J, Buzón V, Maynar P and García de Soria M 2015 *Phys. Rev. E* **91** 052201
[156] Brilliantov N V and Pöschel T 2004 *Kinetic Theory of Granular Gases* (Oxford University Press) (https://doi.org/10.1093/acprof:oso/9780198530381.001.0001)
[157] Chapman S and Cowling T G 1990 *The Mathematical Theory of Non-Uniform Gases: An Account of the Kinetic Theory of Viscosity, Thermal Conduction and Diffusion in Gases* (Cambridge University Press)
[158] Pinto-Goldberg M and Soto R 2025 arXiv:2506.17509
[159] Chapman S 1912 *Phil. Trans. R. Soc. A* **211** 433
[160] Enskog D 1917 *Kinetische Theorie der Vorgänge in mäSsig VerdüNnten Gasen…* vol 1 (Almquist & Wiksell)
[161] Dorfman J R, van Beijeren H and Kirkpatrick T R 2021 *Contemporary Kinetic Theory of Matter* (Cambridge University Press) (https://doi.org/10.1017/9781139025942)
[162] Brey J J, Moreno F and Dufty J W 1996 *Phys. Rev. E* **54** 445
[163] Gómez González R and Garzó V 2022 *Phys. Rev. E* **106** 064902
[164] Hansen J-P and McDonald I R 2013 *Theory of Simple Liquids: With Applications to Soft Matter* (Academic)
[165] McNamara S 1993 *Phys. Fluids A* **5** 3056
[166] Van Noije T, Ernst M, Trizac E and Pagonabarraga I 1999 *Phys. Rev. E* **59** 4326
[167] Nise N S 2020 *Control Systems Engineering* (Wiley)
[168] Durán-Olivencia M A, Yatsyshin P, Goddard B D and Kalliadasis S 2017 *New J. Phys.* **19** 123022
[169] De Zarate J M O and Sengers J V 2006 *Hydrodynamic Fluctuations in Fluids and Fluid Mixtures* (Elsevier)
[170] Vázquez F and Haro M L d 2001 *J. Non Equilib. Thermodyn.* **26** 279
[171] Landau L, Lifshitz E, Landau L and Lifschitz E 1980 *ZAMM Z.* **61** 603
[172] Puglisi A 2017 *Phys. Rev. Lett.* **119** 208003

J. Stat. Mech. (2025) 123206

[173] Manacorda A 2018 *Lattice Models for Fluctuating Hydrodynamics in Granular and Active Matter* (Springer) (https://doi.org/10.1007/978-3-319-95080-8)
[174] Lasanta A, Manacorda A, Prados A and Puglisi A 2015 *New J. Phys.* **17** 083039
[175] Bixon M and Zwanzig R 1969 *Phys. Rev.* **187** 267
[176] Brey J J, Maynar P and Garcia de Soria M 2009 *Phys. Rev. E* **79** 051305
[177] Maynar P, Soria M d and Trizac E 2009 *Eur. Phys. J. Spec. Top.* **179** 123
[178] Bixon M, Dorfman J and Dufty J W 1989 *J. Phys. Chem.* **93** 7019
[179] Bouchet F 2020 *J. Stat. Phys.* **181** 515
[180] Gradenigo G, Sarracino A, Villamaina D and Puglisi A 2011 *J. Stat. Mech.* 08017
[181] Lei Y and Ni R 2024 *J. Phys.: Condens. Matter* **37** 023004
[182] Kuroda Y and Miyazaki K 2023 *J. Stat. Mech.* 103203
[183] Mukherjee A, Tapader D, Hazra A and Pradhan P 2024 *Phys. Rev. E* **110** 024119
[184] Hazra A, Mukherjee A and Pradhan P 2025 *J. Stat. Mech.* 023201
[185] Mkhonta S K, Huang Z-F and Elder K R 2024 *Phys. Rev. Mater.* **8** 104002
[186] Anand S, Zhang G and Martiniani S 2025 arXiv:2505.22933
[187] Grinstein G, Lee D-H and Sachdev S 1990 *Phys. Rev. Lett.* **64** 1927
[188] Garrido P L, Lebowitz J L, Maes C and Spohn H 1990 *Phys. Rev. A* **42** 1954
[189] Plati A and Puglisi A 2021 *Sci. Rep.* **11** 14206
[190] Simha R A and Ramaswamy S 2002 *Phys. Rev. Lett.* **89** 058101
[191] Kundu A, Hirschberg O and Mukamel D 2016 *J. Stat. Mech.* 033108
[192] Spohn H 1983 *J. Phys. A: Math. Gen.* **16** 4275
[193] Dorfman J, Kirkpatrick T and Sengers J 1994 *Annu. Rev. Phys. Chem.* **45** 213
[194] Grinstein G 1991 *J. Appl. Phys.* **69** 5441
[195] Bak P 1992 *Physica A* **191** 41
[196] Giusfredi M, Iubini S and Politi P 2024 *J. Stat. Phys.* **191** 119
[197] Bonachela J A and Munoz M A 2009 *J. Stat. Mech.* 09009
[198] Maire R and Plati A 2024 *J. Chem. Phys.* **161** 054902
[199] Kuroda Y, Kawasaki T and Miyazaki K 2025 *Phys. Rev. Res.* **7** L012048
[200] Galliano L, Cates M E and Berthier L 2023 *Phys. Rev. Lett.* **131** 047101
[201] Keta Y-E and Henkes S 2025 *Soft Matter* **21** 5710–9
[202] Chaikin P M, Lubensky T C and Witten T A 1995 *Principles of Condensed Matter Physics* vol 10 (Cambridge University Press)
[203] Landau L and Placzek G 1934 *Phys. Z. Sowjetunion* **5** 172
[204] Puglisi A, Gnoli A, Gradenigo G, Sarracino A and Villamaina D 2012 *J. Chem. Phys.* **136** 014704
[205] Sarracino A, Villamaina D, Costantini G and Puglisi A 2010 *J. Stat. Mech.* P04013
[206] Spohn H 2014 *J. Stat. Phys.* **154** 1191
[207] Spohn H 2016 *Thermal Transport in Low Dimensions: From Statistical Physics to Nanoscale Heat Transfer* (Springer) p 107
[208] Eltohfa M, Wang X, Griffin C M and Robicheaux F 2024 *Phys. Rev. E* **110** 014114
[209] Moško M and Cambel V 1995 *Acta Phys. Pol. A* **87** 157
[210] Onorato M, Lvov Y V, Dematteis G and Chibbaro S 2023 *Phys. Rep.* **1040** 1
[211] Guzmán M and Soto R 2018 *Phys. Rev. E* **97** 012907
[212] Risso D, Soto R and Guzmán M 2018 *Phys. Rev. E* **98** 022901
[213] Argentina M, Clerc M and Soto R 2002 *Phys. Rev. Lett.* **89** 044301
[214] Chiu Y-J, Evans D and Omar A K 2024 Theory of nonequilibrium multicomponent coexistence (arXiv:2409.07620 [cond-mat.stat-mech])
[215] Solon A P, Stenhammar J, Wittkowski R, Kardar M, Kafri Y, Cates M E and Tailleur J 2015 *Phys. Rev. Lett.* **114** 198301
[216] Solon A P, Stenhammar J, Cates M E, Kafri Y and Tailleur J 2018 *New J. Phys.* **20** 075001
[217] Omar A K, Row H, Mallory S A and Brady J F 2023 *Proc. Natl Acad. Sci.* **120** e2219900120
[218] Feng J and Omar A K 2024 Theory for the anomalous phase behavior of inertial active matter (arXiv:2407.08676 [cond-mat.soft])

J. Stat. Mech. (2025) 123206